

Toward a Deterministic Model of Planetary Formation VI:

Dynamical Interaction and Coagulation of Multiple Rocky Embryos and Super-Earth Systems around Solar Type Stars

S. Ida

Tokyo Institute of Technology, Ookayama, Meguro-ku, Tokyo 152-8551, Japan

`ida@geo.titech.ac.jp`

and

D. N. C. Lin

UCO/Lick Observatory, University of California, Santa Cruz, CA 95064

Kaoli Institute for Astronomy and Astrophysics, Peking University, Beijing, China

`lin@ucolick.org`

ABSTRACT

Radial velocity and transit surveys indicate that solar-type stars bear super-Earths, with mass and period up to $\sim 20M_{\oplus}$ and a few months, are more common than those with Jupiter-mass gas giants. In many cases, these super-Earths are members of multiple-planet systems in which their mutual dynamical interaction has influenced their formation and evolution. In this paper, we modify an existing numerical population synthesis scheme to take into account protoplanetary embryos' interaction with their evolving natal gaseous disk, as well as their close scatterings and resonant interaction with each other. We show that it is possible for a group of compact embryos to emerge interior to the ice line, grow, migrate, and congregate into closely-packed convoys which stall in the proximity of their host stars. After the disk-gas depletion, they undergo orbit crossing, close scattering, and giant impacts to form multiple rocky Earths or super-Earths in non-resonant orbits around $\sim 0.1\text{AU}$ with moderate eccentricities of $\sim 0.01\text{--}0.1$. We suggest that most refractory super-Earths with period in the range of a few days to weeks may have formed through this process. These super-Earths differ from Neptune-like ice giants by their compact sizes and lack of a substantial gaseous envelope.

Subject headings: planetary systems: formation – solar system: formation – stars: statics

1. Introduction

In the past decade, more than 400 extrasolar planets have been discovered around nearby solar-type stars. Most of these known planets are probably gas giants because they have masses (M_p) and densities (ρ_p) comparable to those of Jupiter and Saturn, while their periods (P) ranges from a few days to years. When this population is extrapolated to longer periods (more than a decades), their ubiquity implies that the fraction of solar-type stars which have gas giant planets around them is approximately $\eta_J \sim 10\text{--}15\%$ (Cumming et al. 2008).

Gas giant planets must formed in gas-rich environment. However, in contrast to the modest value of η_J , the T Tauri progenitors of solar-type stars are commonly surrounded by protostellar disks (Beckwith & Sargent 1996) with surface densities comparable to that of the minimum mass solar nebula model (MMSN) (Hayashi 1981). Based on the conventional paradigm that gas giant planets form in frequently-observed, evolving, natal protostellar disks through the condensation of grains, coagulation of planetesimals, mergers of protoplanetary embryos, and gas accretion onto super-Earth (with masses in excess of a few Earth-masses) cores, we constructed a population-synthesis model through a series of papers (Ida & Lin 2004a,b, 2005, 2008a,b, , hereafter Papers I-V). In these papers, we qualitatively showed that the low fertility rate of gas giants (*i.e.*, the modest value of η_J) around solar type stars despite the omnipresence of planetary cradles around their progenitor T Tauri stars is due to 1) an inefficient retention of building-block materials in protostellar disks and 2) that gas giant planet formation is only possible in relatively-massive (super-MMSN) protostellar disks which deplete on time scales (τ_{dep}) longer than ~ 3 Myr.

The observed mass-period ($M_p - P$) distribution of these planets appear to be non-uniform (Ward 1986; Cumming et al. 2008). With a set of well-define and carefully-selected sample, potential observational selection effects may be quantitatively identified and taken into account (Schlaufman et al. 2009). Analogous to the stellar color-magnitude diagram for galactic and globular clusters, genuine oasis and deserts in planets' $M_p - P$ distribution of a controlled samples can be used to cast constraints and provide clues to the theory of planet formation and planetary-system evolution.

Preliminary results of our first sets of simulations essentially reproduced known-planets' observed $M_p - P$ distribution and the fraction of planet-bearing stars as a function of their mass and metallicity (Papers II and III). They have also been reproduced and confirmed by similar population-synthesis approaches (Mordasini et al. 2009) and hybrid (N-body + 1D viscous-disk evolution) simulations (Thommes et al. 2008a), albeit there remain some differences in the asymptotic $M_p - P$ distribution. Nevertheless the statistical significance of these agreements remain unsettled, because 1) existing observational data are acquired with heterogeneous precession and diverse observational selection criteria and 2) theoretical frameworks of some critical physical processes remain poorly understood. Ideally, the construction and upgrades of population-synthesis models can be used 1) to set quantitative calibrations on important model parameters and 2) to extrapolate tests and predictions for subsequent observations.

In our previous five papers, quantitative determination of the efficiency of gas giant formation around different types of host stars, many uncertainties remain in the prescriptions adopted for these models. They include the magnitude of the following input parameters as defined in paper IV:

- 1) the surface density distribution of gas (the fiducial magnitude Σ_g or $f_{g,0}$ and power index q_g as defined in Eq. [1] below), effective viscosity (ν or the dimensionless α parameter) as a function of radius r (see Paper V), mass-flow rate (\dot{M}_{disk}) and depletion time scale τ_{dep} of the disk gas (as defined Paper I),
- 2) the surface density distribution of solid building-block (grains, planetesimals, and protoplanetary embryos) material (the fiducial magnitude Σ_d or f_d and power index q_d as defined in Eq. [1]),
- 3) the scaling coefficients (h_d and h_g as defined in Papers II and III) of dust and gas contents in the disk associated with a range of the stellar mass (M_*) and metallicity ($[\text{Fe}/\text{H}]$),
- 4) the rate of type-I migration of protoplanetary embryos which is characterized by a parameter C_1 in comparison with the linear calculation for unperturbed disks (see Paper IV),
- 5) the stalling process and location of both type I and II migration, and
- 6) the rate of gas accretion onto protoplanetary cores (which is characterized by k_1 and k_2 in Paper I).

These properties are determined by the not-so-well understood physical processes such as the efficiency of turbulent angular momentum transport (items 1 & 3) and retention of heavy elements in the form of grains (items 2 & 3), planetesimals, and embryos (items 4 & 5). With regard to item 6, in the sequential accretion hypothesis, the formation of gas giants must be preceded by the emergence of cores with several M_{\oplus} 's (Mizuno 1980; Pollack et al. 1996; Ikoma et al. 2000). These uncertainties are not independent of each other. In particular, the fraction of solar-type stars which bear gas giants depends on the inventory of building block material and the retention efficiency of cores. In Paper IV, we demonstrated that in disks with power-law Σ_g and Σ_d distributions, the observed η_J would be achievable only if 1) the disk is more massive than the MMSN model (*i.e.* $f_d \gtrsim 1$), and 2) type I migration is relatively inefficient (*i.e.* $C_1 \lesssim 0.03$).

These requirements need not be satisfied throughout the disk provided there are special locations in the disk where building-block grains can accumulate and embryos' type I migration may be suppressed (see Paper V). In this context, the ice line appears to be a preferred birth place for gas giants because it provides a natural barrier against the orbital decay of grains (due to hydro dynamic drag) and protoplanetary embryos (due to type I migration) (Kretke & Lin 2007). The period distribution of the simulated models which take into account of the preferred birth place of gas giants (Paper V) can match well with a conspicuous (2-3 yrs) up-turn in observed period distributions of Jupiter-mass planets provided $C_1 \sim 0.1$ (Schlaufman et al. 2009).

Ongoing transit searches and high-precision radial velocity surveys have led to the discovery of

many short-period (with P less than a week) gas giants. According to the population synthesis models, these planets relocated to their present-day orbit either through type II migration or dynamical instability and relaxation. For this scenario, we need to verify: 1) criteria for gas giants’ relocation shortly after their formation, 2) efficiency of relocation processes, 3) condition for stalling dynamical evolution, and 4) extent of gas giants’ mass loss and orbital decay during the main sequence life span of their host stars. Through detailed quantitative comparisons between population-synthesis models and observational data, we can calibrate the efficiency of various relevant and competing processes.

In addition to the reproduction of known observational properties (mostly for gas giants), population-synthesis models may also be used to make some robust predictions. A particularly noticeable feature in the simulated $M_p - P$ distribution is a domain of planetary desert for intermediate mass ($\sim 20 - 100M_\oplus$) and period (weeks to months) planets with comparable gas and solid internal composition. While the actual boundaries of this parameter region depend on the values of various input parameters (such as k_1 , k_2 , C_1 etc), the paucity of planets in this domain is robust, mainly due to the combined effects of runaway gas accretion (Paper I) and type I migration (Paper IV). This region of parameter space would be filled if the gas accretion onto the cores is significantly slowed down by inefficient heat transfer in the infalling envelope or type I migration is grossly inhibited everywhere in the case where planetesimal accretion of migrating cores is not inhibited (Mordasini et al. 2009). Thus, forthcoming observations can be used to distinguish key assumptions associated with these models.

In the context of quantitative predictions, the simulated planet distribution also highlights rich populations of both Earth-mass rocky planets and long-period ice giants. During the early epochs of disks’ evolution (especially when they undergo repeated FU Ori outbursts), \dot{M}_{disk} , Σ_g and Σ_d are much larger than their values in the MMSN model. In principle, embryos can rapidly undergo oligarchic growth (Kokubo & Ida 1998, 2002) and attain isolation masses $M_{c,\text{iso}}$ which are sufficiently large ($\sim 3 - 10M_\oplus$) to initiate dynamical gas accretion exterior to the ice line (Paper I). However, even with a modest amount of type I migration (*i.e.* $C_1 \sim 10^{-2}$), the embryos would migrate towards their host stars before they reach their isolation masses (Paper IV). In inner regions at $\lesssim 0.5\text{AU}$, the surface density of rocky materials is severely depleted by type I migration of embryos that start migration after they acquire mass comparable to their isolation mass (Paper IV).

The fate of these embryos is determined by their retention probability. If they are efficiently retained, they would emerge as conspicuous super-Earths. In contrast to gas giants’ type II migration, embryos’ type I migration and retention processes in the proximity of their host stars are poorly understood. In Papers I-V, we counted the number of embryos (with different masses) which are expected to cross some inhibited inner disk boundary.

In this paper, we consider various physical processes which may regulate embryos’ dynamical evolution and determine the formation and retention probability of super-Earths at various

locations. This follow-up study is timely because recent radial-velocity surveys with high-cadence (several times nightly) and precision (down to \sim m/s) have led to the announced discoveries of several super-Earths with masses and periods up to $\sim 20M_{\oplus}$ and a few months (Mayor *et al.* 2009). These data also suggest super-Earths may exist around nearly half of all nearby solar-type stars and in many cases in the form of non-resonant multiple-planet systems (M. Mayor, S. Udry, private communication). This trend, when confirmed with a well-defined controlled sample, would suggest there may be many Earth-mass or sub-Earth slowly-growing cores which failed to accrete any significant amount of gas before their natal disk is evaporated. They also highlight the importance of dynamical interaction between multiple embryos during their formation and subsequent evolution.

In order to analyze the asymptotic evolution of multiple-embryo systems, we briefly summarize, in §2, some relevant physical processes and introduce a set of generic prescriptions which can be reliably used to quantitatively approximate embryos' interaction with each other and their natal disks. In §3, we utilize this prescription, along with our previously established algorithms, to carry out some case studies for formation of multiple rocky/icy planetary systems around a majority of solar type stars which do not bear any gas giant planets. Based on the results of Paper I and IV, we suggest these planets formed in relatively low or modest mass disks. These disks generally have gas surface density (Σ_g) less than 2-3 times that of the minimum mass solar nebula (MMSN) model. We show that prior to gas depletion, dynamically isolated embryos emerge with sub-Earth masses and nearly circular orbits in the inner parts of these disks (*i.e.* interior to the ice line). We refer to this first epoch as the embryos-emergence stage.

During the (second) migration and accumulation stage, these embryos rapidly migrate to proximity of their host stars. Under various circumstances, embryos' migration may be stalled in the inner regions of disks around classical T Tauri stars. After the gas depletion, the congregated embryos perturb each other's orbits. Within the next ~ 100 Myr, dynamical instability induces embryos to cross each other's orbits and growth through cohesive collisions. During this (third) giant impact stage, super-Earths form with periods between a few days to months and modest eccentricities ($e \sim 0.01$ – 0.1). As the host stars mature, inelastic and cohesive collisions between embryos with modest relative periapse longitudes damp their eccentricities. In the absence of gas giants, systems eventually evolve into a (fourth) stabilizing state in which the residual planets' crossing timescale becomes larger than the age of the system. We show that these models naturally account for the origin of a known population of non-resonant multiple Earth/super-Earth systems with periods ranging from days to months. The asymptotic mass of some planets may exceed that (several Earth masses) needed to initiate efficient gas accretion in a MMSN environment. But these planets acquired most of their masses through giant impacts after the gas is depleted from their natal disks. In the absence of gas accretion, such super-Earths do not evolve into gas giants. Finally, we summarize our results and discuss their implications in §4.

2. Embryos interaction with each other and their natal disks

The main difference between the present investigation and that in papers I-V are: 1) the inclusion of resonant capture between embryos during type I migration, and 2) the calculation of embryos’ orbital and mass evolution after the gas depletion. These effects are important for the formation of multiple Earths and super-Earth systems through collisional merger (giant impact) events. We describe in this section some modification and additions to our method of treating these interactions.

2.1. Disk models

Although disk gas accretion rates in the inner regions and the surface density of dust in the outermost regions of protostellar disks have been observationally inferred, there are no reliable observational constraints on the gas and heavy-element surface density distribution especially near the planet forming regions. Theoretical determination of these quantities relies on poorly determined magnitude of angular momentum transfer efficiency.

In light of this uncertainty, we adopt the MMSN model (Hayashi 1981) as a fiducial set of initial conditions. In our population-synthesis model, we introduce multiplicative factors (f_d and f_g) to scale the disk surface densities of gas (Σ_g) and planetesimals (Σ_d) with those of the MMSN model. Following Paper IV, we set

$$\begin{cases} \Sigma_d &= \Sigma_{d,10} \eta_{\text{ice}} f_d (r/10\text{AU})^{-q_d}, \\ \Sigma_g &= \Sigma_{g,10} f_g (r/10\text{AU})^{-q_g}, \end{cases} \quad (1)$$

where normalization factors $\Sigma_{d,10} = 0.32\text{g/cm}^2$ and $\Sigma_{g,10} = 75\text{g/cm}^2$ correspond to 1.4 times of Σ_g and Σ_d at 10AU of the MMSN model, and the step function $\eta_{\text{ice}} = 1$ inside the ice line at a_{ice} (eq. [3]) and 4.2 for $r > a_{\text{ice}}$ [the latter can be slightly smaller (~ 3.0) (Pollack et al. 1994)].

In Paper V, we considered disk evolution with constant α and the ice line barrier for migration (a local Σ_g maximum is due to a transition in the thickness of MRI active layers across the ice line). In this paper, we use a simple power-law disk model in order to focus our attention on the effects of dynamical interactions that we now take into consideration in our sequential planet formation model. Nevertheless, we specify an inner disk boundary where Σ_g vanishes and planetesimals’ type I migration is arrested (see §2.5).

Neglecting the detailed energy balance in the disk (Chiang & Goldreich 1997; Garaud & Lin 2007), we adopt the equilibrium temperature distribution of optically thin disks prescribed by Hayashi (1981) such that

$$T = 280 \left(\frac{r}{1\text{AU}} \right)^{-1/2} \left(\frac{L_*}{L_\odot} \right)^{1/4} \text{K}, \quad (2)$$

where L_* and L_\odot are stellar and solar luminosity. In this simple prescription, we set the ice line to

be that determined by an equilibrium temperature (eq. [2]) in optically thin disk regions,

$$a_{\text{ice}} = 2.7(L_*/L_\odot)^{1/2}\text{AU}. \quad (3)$$

The magnitude of a_{ice} may be modified by the local viscous dissipation (Lecar et al. 2006) and stellar irradiation (Chiang & Goldreich 1997; Garaud & Lin 2007). The evolution of the ice line may affect frequency of gas giant planets around high-mass stars (Kennedy et al. 2006; Kennedy & Kenyon 2008). These potentially important effects will be incorporated in subsequent papers.

Dependence of disk metallicity is attributed to distribution of $f_{d,0} = f_{g,0}10^{[\text{Fe}/\text{H}]_d}$, where $f_{d,0}$ and $f_{g,0}$ are initial values of f_d and f_g , respectively. Due to viscous diffusion and photoevaporation, f_g decreases with time. For simplicity, we adopt

$$f_g = f_{g,0} \exp(-t/\tau_{\text{dep}}), \quad (4)$$

where τ_{dep} is disk lifetime (for detailed discussion, see Paper IV). The constant α self-similar solution obtained by Lynden-Bell & Pringle (1974) is expressed by $\Sigma_g \propto r^{-1}$ with an asymptotic exponential cut-off at radius r_0 of the maximum viscous couple. In the region at $r < r_0$, Σ_g decreases uniformly independent of r as the exponential decay does, although the time dependence is different. In the self-similar solution, Σ_g at $r < r_0$ decays as $\Sigma_g \propto (t/\tau_{\text{dep}} + 1)^{-3/2}$. In the exponential decay model that we adopt, Σ_g decays more rapidly as t/τ_{dep} becomes larger at $t > \tau_{\text{dep}}$. If the effect of photoevaporation is taken into account, Σ_g decays rapidly after it is significantly depleted, so that the exponential decay mimics the effect of photoevaporation. We also carried out some runs with $\Sigma_g \propto (t/\tau_{\text{dep}} + 1)^{-3/2}$, but we did not find any significant difference in the results from the exponential decay cases. In the population synthesis models in Papers I-V, a log uniform distribution in a range of 10^6 – 10^7 yrs was adopted for τ_{dep} . In the present paper, we fix the value τ_{dep} to be 3×10^6 yrs.

2.2. From Oligarchic Growth to Isolation

On the basis of oligarchic growth model (Kokubo & Ida 1998, 2002), growth rate of embryos/cores at any location a and time t in the presence of disk gas, is described by $dM_c/dt = M_c/\tau_{c,\text{acc}}$ where, after correcting some typos in Paper IV,

$$\tau_{c,\text{acc}} = 2.2 \times 10^{5-q'_d-(2q'_g/5)} \eta_{\text{ice}}^{-1} f_d^{-1} f_g^{-2/5} \left(\frac{a}{1\text{AU}}\right)^{(27/10)+q'_d+(2q'_g/5)} \left(\frac{M_c}{M_\oplus}\right)^{1/3} \left(\frac{M_*}{M_\odot}\right)^{-1/6} \text{yrs}, \quad (5)$$

M_c is the mass of the embryo (core), $q'_d = q_d - 3/2$ and $q'_g = q_g - 3/2$, and we have adopted the mass of the typical field planetesimals to be $m = 10^{20}\text{g}$.

Embryos' gravitational perturbations continually excite the eccentricity of the field planetesimals. Prior to the gas depletion, planetesimals' eccentricity is also damped by hydrodynamic drag

so that embryos’ growth is enhanced by their gravitational focusing effect. In this limit, the full width of feeding zone of an embryo with a mass M_c is given by (Kokubo & Ida 1998, 2002)

$$\Delta a_c = 10r_H = 10 \left(\frac{2M_c}{3M_*} \right)^{1/3} a, \quad (6)$$

where r_H is two-body Hill radius. In situ growth of embryos is quenched when they acquire all the heavy-element building block material within their feeding zone. The maximum mass (called isolation mass) of immobile embryos in oligarchic growth stage is given by (Kokubo & Ida 1998, 2002)

$$M_{c,\text{iso}} \simeq 0.16 \eta_{\text{ice}}^{3/2} f_d^{3/2} \left(\frac{a}{1\text{AU}} \right)^{3/4 - (3q'_d/2)} \left(\frac{M_*}{M_\odot} \right)^{-1/2} M_\oplus. \quad (7)$$

In Papers I-V, we adopted the above formulae for mass accretion timescale during the oligarchic growth in the presence of disk gas. We also assumed that after the gas depletion embryos’ and planetesimals’ velocity dispersion becomes comparable to surface escape velocity of the most massive embryos at that location. This kinematic transition widens embryos’ feeding zone which enable them to acquire more planetesimals and attain larger asymptotic masses, though at slower rates (because their collisional cross section is reduced to their geometric surface area).

In these previous first-attempt approximations, each embryo was treated separately and their mutual interaction was neglected. For example, in Papers IV and V, decreases in Σ_d due to accretion by independent planetary embryos are computed only in the feeding zones centered around their original locations. But, in the presence of disk gas, embryos undergo type I migration due to imbalance in the tidal torques from outer and inner disks (see §2.3). Relocation to regions with different surface densities (which is also depleted by previous generation of embryos) would modify embryos’ growth rate and asymptotic mass. In order to take into account the possibility of growth along migration path, we adopted, in our previous papers, a prescription that embryos’ growth rate is determined by the same value of f_d in their original feeding zone until the migrating embryos reach the empirically-derived critical radius ($a_{\text{dep,mig}}$) within which the residual planetesimals are totally emptied by the preceding migrating embryos. This awkward scheme was introduced for computational convenience. In the context of gas-giant formation, embryos evolve into dynamically isolated cores with nearly circular orbits in gaseous environment. This approximation is adequate for the evaluation of their individual growth and migration. It is also reasonable to assume Σ_d is depleted in this inside-out manner without the consideration of any competitive neighbors.

In the present paper, however, we intend to determine the mass spectrum and kinematic distribution of multiple planetary systems around common host stars. Here, we need to consider the concurrent disk evolution along with the mass and dynamical evolution of several coexisting embryos in evolving disks (see below and §2.3). Under some circumstances, it is possible for the Σ_d decline to be a non monotonic function of a . (For example, the emergence of relatively massive embryos across the ice line can lead to the formation of “gaps” in the Σ_d distribution.) In order to take this possibility into account, we compute the evolution of Σ_d distribution due to accretion by

all the emerging embryos in a self-consistent manner.

In our newly modified scheme, the growth and migration of several embryos are integrated simultaneously with the evolution of the Σ_d -distribution. We set up linear grids for f_d across the disk with typical width of $\sim 10^{-3}$ AU. We introduce a population of seed embryos, all with an initial mass 10^{20} g (*i.e.* that of the residual planetesimals) and compute their mass accretion rate. In the inner disk region (interior to the ice line), we set the initial separation of these seed planetesimals at any given location a_0 to be the full feeding-zone width ($\Delta a_c = 10r_H$) of embryos with local asymptotic isolation mass $M_{c,iso}$. We justify this prescription on the basis that in location where $\tau_{c,acc}(M_{c,iso}) < \tau_{dep}$, any seed embryos with closer initial separations would have merged and additional embryos would have formed unless the entire disk is filled with isolated embryos. Thus, this choice of seed planetesimals is optimized for computational efficiency, without the loss of completeness.

In the outer disk region where embryos' growth is slow, they are unlikely to attain a local isolation masses within the life span of their host stars. A more realistic estimate for their asymptotic mass is that (M_9) inferred from equation (5) for the local Σ_d after $t \sim 1$ Gyr. In the same spirit of optimizing computational efficiency without introducing incompleteness, we place seed embryos with an initial separation which corresponds to Δa_c (full feeding zone width) of embryos with mass M_9 . For intermediate disk region, the initial spacing for the seed embryos is chosen to be Δa_c for the minimum value of $M_{c,iso}$ and M_9 . Provided there is a sufficient supply of seed planetesimals, our results do not depend on the choice of their initial spacing.

We follow the growth of the seed embryos due to planetesimal accretion in accordance with Equations (5) and (6). The planetesimals' mass accreted by the embryos is uniformly subtracted from the grids that are covered by their instantaneous Δa_c appropriate for their current mass and location. (For example, the feeding zone of an Earth-mass planet at 1AU extends over 100 numerical grid points in the Σ_d distribution.) We follow the evolution of Σ_d in each individual grids and use their values to evaluate embryos' accretion rate and the strength of dynamical friction from the planetesimals. With this treatment, we no longer need to assume some empirical values for Σ_d and $a_{dep,mig}$ in the evaluation of migrating embryos' accretion rate.

Embryos formed through oligarchic growth attain isolation mass and are well-separated ($\sim \Delta a_c$) from each other. Despite their mutual gravitational perturbation, tidal drag from disk gas (Artymowicz 1993; Ward 1993) and dynamical friction from planetesimals (e.g., Stewart & Ida 2000) are sufficiently strong to generally preserve embryos' circular orbits. Consequently, the stability of these widely separated embryos is well preserved (Iwasaki et al. 2002). In our prescription, the process of embryos' oligarchic growth in a gas-rich environment is adequately represented by planetesimal accretion onto initially well-separated seed embryos. Nevertheless, embryos' mutual perturbation may become important if their orbits evolve and masses grow beyond isolation (see §2.6).

2.3. Type I migration

The growing embryos exert tidal torque on their natal disks. With sufficient masses, they undergo generally-inward type I migration (Goldreich & Tremaine 1982; Ward 1986; Tanaka et al. 2002). Several numerical simulations have shown that type I migration can be retarded in turbulent disks (Laughlin et al. 2004; Nelson 2005; Baruteau & Lin 2010) and weakly viscous or inviscid laminar disks (Koller et al. 2003; Li et al. 2009). The effect of corotation torque and horseshoe drag can also reduce the rate and change the direction of migration in disks with various Σ_g and T distributions (Masset & Casoli 2009; Paardekooper et al. 2010). But, the efficiency of these effects depends on the turbulent induced angular momentum and heat diffusion coefficients.

A detailed study of the type I migration is beyond the scope of this paper. However, we can utilize our population synthesis models to calibrate the relative importance of several competing effects. In this paper, we follow the prescription in Paper IV and use the formula for the migration rate that was derived through 3D linear calculation (Tanaka et al. 2002):

$$\begin{aligned} \tau_{\text{mig1}} &= \frac{a}{\dot{a}} = \frac{1}{C_1} \frac{1}{2.728 + 1.082q_g} \left(\frac{c_s}{a\Omega_K} \right)^2 \frac{M_*}{M_p} \frac{M_*}{a^2 \Sigma_g} \Omega_K^{-1} \\ &\simeq 5 \times 10^4 \times 10^{-q'_g} \frac{1}{C_1 f_g} \left(\frac{M_c}{M_\oplus} \right)^{-1} \left(\frac{a}{1\text{AU}} \right)^{q_g} \left(\frac{M_*}{M_\odot} \right)^{3/2} \text{ yrs.} \end{aligned} \quad (8)$$

where C_1 is a free parameter for the retardation of migration, reflecting possible non-linear effects including turbulence (see Paper IV). The expression of Tanaka et al. (2002) corresponds to $C_1 = 1$, and for slower migration, $C_1 < 1$. It also neglects the effect of horseshoe torque associated with either Σ_g and T distribution. The implication of these effects on the formation of planets and planetary systems will be addressed in the next paper together with that associated with a migration barrier at the inner boundary of global dead zone.

In this paper, we are primarily interested in planetary systems without gas giants. Equations (5) and (7) indicate that on a time scale $\sim \tau_{\text{dep}}$, the most massive embryos emerge from relatively low-mass disks (with $f_g = f_d \sim 1$) attain masses a few times that of the Earth. Although these embryos (or equivalently cores) can accrete gas, it forms slowly contracting envelopes with insignificant masses (Paper I). For the case studies in §3, we assume that prior to gas depletion, all embryos have sub-critical masses $\lesssim 3 - 10M_\odot$ and neglect their gas accretion.

Orbital migration relocates embryos to regions with fresh supplies of residual planetesimals. It can also lead embryos to regions where planetesimals are severely depleted by the prior accretion of other embryos. Equations (5) and (6) are formulae for oligarchic growth stage. They indicate that both \dot{M}_c and $M_{c,\text{iso}}$ depend on embryos' local Σ_d . In our numerical scheme, we compute the instantaneous local \dot{M}_c and $M_{c,\text{iso}}$ of migrating embryos together with the evolution of Σ_d (see §2.2).

2.4. Resonant capture

In intermediate-mass disks (with $1 \lesssim f_g \lesssim 3$), some embryos form with super-Earth masses. Even with a ten-fold reduction in efficiency (with $C_1 \sim 0.1$), these massive embryos undergo type-I migration over significant distances from the ice line prior to the gas depletion. Embryos' relocation also provides an opportunity to replenish their feeding zone and to grow beyond their initial isolation mass. Differential type I migration can reduce (as well as widen) the orbital separation between some embryos.

Embryos with converging orbits may also capture each other into mean-motion resonances. After they enter resonances, these embryos have a tendency to migrate together while maintaining the ratio of their semimajor axes. N-body simulations (McNeil et al. 2005; Ogihara & Ida 2009) illustrate the possible formation of migrating convoys with several resonant embryos. In order to construct an utilitarian prescription for resonant capture, we first compute the rate of type I migration for each coexisting embryos separately and independently. We identify convergent pairs (i, j) from their differential migration speed. Next, we consider dynamical perturbation between embryos of closest pairs (i, j) . Neglecting perturbation by other more distant embryos, their orbital separation ($b = |a_i - a_j|$) expands impulsively after each conjunction. For nearly circular orbits, the expansion of embryos' spacing after an encounter is given by a linear analysis (Goldreich & Tremaine 1982; Hasegawa & Nakazawa 1990) as

$$\delta b \simeq 30 \left(\frac{b}{r_H} \right)^{-5} r_H, \quad (9)$$

where $r_H = ((m_i + m_j)/3M_*)^{1/3}a$. Since encounters occur at every synodic period [$T_{\text{syn}} = 2\pi a / ((d\Omega/da)b) \simeq (4\pi a / 3b\Omega_K)$], we find the changing rate to be

$$\frac{db}{dt} \simeq \frac{\delta b}{T_{\text{syn}}} \simeq 7 \left(\frac{b}{r_H} \right)^{-4} \left(\frac{r_H}{a} \right)^2 v_K. \quad (10)$$

In the limit that db/dt becomes comparable to the differential type I migration speed, $\Delta v_{\text{mig}} = v_{\text{mig},i} - v_{\text{mig},j}$, convergent embryos' mutual interaction would be compensated by their relative motion (with speeds $v_{\text{mig},i}$ and $v_{\text{mig},j}$ respectively). In this equilibrium, the separation of two convergent embryos would be maintained at

$$b_{\text{trap}} \simeq 0.16 \left(\frac{m_i + m_j}{M_\oplus} \right)^{1/6} \left(\frac{\Delta v_{\text{mig}}}{v_K} \right)^{-1/4} r_H. \quad (11)$$

For computational simplicity, we set $v_{\text{mig},i} = a/\tau_{\text{mig},i}$ where $\tau_{\text{mig},i}$ (for an embryos with a mass m_i) is given by equation (8),

$$b_{\text{trap}} \simeq 4 \times 10^{-q'_g/4} \left(\frac{m_i + m_j}{M_\oplus} \right)^{-1/12} f_g^{-1/4} C_1^{-1/4} \left(\frac{a}{1\text{AU}} \right)^{q'_g/4} \left(\frac{M_*}{M_\odot} \right)^{1/4} r_H. \quad (12)$$

In the above expression, dependences of b_{trap} on various parameters are very weak and its magnitude is always $\simeq 4 - 5r_{\text{H}}$.

In the construction of a simple analytic approximation, we assume convergent embryos would capture each other into their low-order main-motion resonance with a semimajor axis separation comparable to b_{trap} . We note that if the estimated value of b_{trap} is smaller than $2\sqrt{3}r_{\text{H}}$, resonant capture would not actually occur, because embryos' separation is within their feeding zone and Δb (in eq. 9) is saturated due to the non-linear effect of overlapping resonances (e.g., Nakazawa & Ida 1988).

The condition for resonant capture is marginally satisfied for embryos which undergo rapid type I migration with $C_1 \sim 1$. In this limit, trapping would be possible if multiple embryos have similar masses and migration speed (so that their relative migration speed is slow). N-body simulations (McNeil et al. 2005; Ogihara & Ida 2009) show that several embryos do migrate together in such cases. However, near the disk inner edge, earliest-generation embryos accumulate as their migration is halted there. When subsequent-generation embryos approach these stalled population with their full migration speed, orbit crossing may occur because b_{trap} is reduced below $4 - 5r_{\text{H}}$. After these embryos undergo dynamical relaxation and cohesive collisions (Terquem & Papaloizou 2007; Ogihara & Ida 2009), several embryos may eventually survive as merger products in some new resonance configuration.

In our numerical scheme, we assume that in the limit of inefficient type I migration (with $C_1 \simeq 0.1$), resonant trapping always occurs at $b_{\text{trap}} = 5r_{\text{H}}$. Even at the disks' inner edge, the separation between stalled resonant Earth-mass embryos is comparable to or larger than the total width of their feeding zones. Resonant embryos which captured each other along their migration paths would spiral towards their host star in lock-step provided their differential tidal torque continues to enforce convergent orbital evolution. During subsequent migration, resonant embryos' eccentricities are excited due to the conservation of an adiabatic invariance (Murray & Dermott 2000). But, they are also effectively damped by embryos' tidal interaction with the disk gas. Interior to the ice line in MMSN-type disks, an equilibrium is established in which the largest (Earth-mass) resonant embryos retain a small amount of non circular motion (Chambers et al. 1996; Zhou et al. 2007). In general, resonant embryos' equilibrium e is less than the ratio of their separation to their semimajor axis $e_b \equiv b/a$ and the resonant embryos' orbits remain dynamically separated.

Based on this consideration, we neglect the possibility of mergers between resonant embryos prior to gas depletion regardless whether they are migrating or stalled near the disks' inner edge. We assume converging embryos capture each other into their low-order main-motion resonances for which their separation is $b_{\text{trap}} \simeq 5r_{\text{H}}$. In our numerical scheme, we monitor the spacing between all migrating embryos. When b between any pairs of resonant embryos is reduced below b_{trap} during orbital integration, we compute, for the next time step, their total angular momentum loss to the disk due to type I migration. This loss is then redistributed among the resonant embryos such that they would migrate together with a fixed spacing $b = 5r_{\text{H}}$ between them.

When resonant embryos migrate to the inner boundary of the disk, they endure a strong corotation torque from the disk gas which halts their orbital decay (see below). This migration barrier is maintained during the subsequent arrival and resonant capture of additional incoming embryos.

2.5. Halting migration in the stellar proximity.

In most inner disk regions (within ~ 1 AU), super-Earth embryos undergo rapid, inward, type I migration. However, at special locations where the gas surface density or entropy attain local maxima, these embryos' type I migration may be stalled due to their tidal interaction with the disk gas near their co-orbital region (Masset et al. 2006; Paardekooper et al. 2010). In MMSN disks, a barrier against type I migration is located at the inner boundary of the 'dead zone' where gas in the disk midplane is totally neutral and not directly affected by magneto-rotational instabilities (Kretke & Lin 2007). However, this barrier moves inward and eventually vanishes during the late stages of disk evolution when Σ_g become sufficiently small for the entire disk to become active (Kretke & Lin 2010). Near both (outer and inner) boundaries of the dead zone, angular momentum transfer by MRI can induce local uniform rotation in the gas flow. The outer part of these rigidly rotation zone attains super-Keplerian flow which also induces a migration barrier (Kato et al. 2009).

Stellar magnetic torque can clear out disk gas inside the radius where it is balanced by viscous stress in the disk (Konigl 1991). In typical protostellar disks, this interaction induces the central stars to co-rotate with the Keplerian frequency at their inner edge. Type I migration may also be halted on the outer boundary of a magnetospheric cavity (Masset et al. 2006). We discuss, in more detail below, a powerful halting mechanism at the outer boundary of the cavity.

In contrast, gas giants induce gap formation in their natal disks and undergo type II migration which is generally inward inside a few AU's (Lin & Papaloizou 1985). Type II migration is generally stalled well inside the magnetospheric cavity. Since gas is severely depleted throughout this magnetospheric cavity, tidal torque between disks and planets well inside the cavity vanishes. In the limit of weak magnetic field, the size of the cavity (r_m) becomes comparable to or smaller than the stellar radii and gas giants may be halted by their tidal interaction with their rapidly rotating host stars (Lin et al. 1996). Although gas giants are shielded and generally not affected by the stellar field directly, it can potentially induce Roche-lobe overflow to halt their inward migration (Laine et al. 2008). Unless their host stars' magnetic and spin axes are aligned, close-in gas giants would be exposed to periodic field modulation and induced current in the upper envelope on their night side where the magnetic diffusivity is relatively large. Ohmic dissipation heats the envelope to induce their Roche-lobe overflow. In either case, gas giants are likely to park closer to their host stars than super-Earths.

Thermal expansion of rocky embryos is generally negligible. However, rocky embryos generally have higher conductivity than the atmosphere of their host stars so that the magnetic flux

tube connecting non-embedded planets and their host stars would slip through the envelope of the host stars much faster than across the planets. The potential drop across the field lines drives a DC current which is analogous to that proposed for the electrodynamics of the Io-Jupiter system (Goldreich & Lynden-Bell 1969). The Ohmic dissipation of this current produces a torque which drives the planet’s orbit to evolve toward a state of circularization and synchronization with the spin of the star. Around slowly (or rapidly) spinning stars, this process can also cause rocky planets with periods less than a few days to undergo orbital decay (or expansion/stagnation) within a few Myr, which can affect the retention efficiency of short-period super earths. This effect is discussed in a separate paper (Laine & Lin 2010). We neglect it in the present paper.

In Papers I-V, we artificially halted type II migration of gas giants and type I migration of rocky/icy embryos at orbital periods of a few days. This prescription was introduced to simulate the effects of an inner cavity in protostellar disks around magnetized T Tauri stars. Using this prescription, we were able to infer a statistical estimate on the fraction of “hot jupiters” among all known gas giant planets. In this paper, we focus our investigation on the stalling mechanism for super-Earths’ type I migration at the outer radius (r_m) of the magnetospheric cavity. Although the transition radius between the dead and active regions is also important for longer-period rocky/icy planets (Kretke & Lin 2010), we will consider this more complex effect in the next paper.

In order to specify a magnitude for r_m , we note that the observed spin periods of young stars show a bimodal distribution at peaks at about one week and one day (Herbst & Mundt 2005)¹. Herbst & Mundt (2005) suggested that for the one-week period stars the stellar magnetic field is coupled with the protostellar disk strongly enough to transfer spin angular momentum to the disk and open up a cavity, while the one-day period stars do not have a cavity. In order to take into account both possibilities, we adopt two different inner boundary conditions: i) with or ii) without cavities.

In models which neglect the presence of magnetospheric cavity, all the embryos that migrate to a radius of 3-day orbital period (0.04AU in the case of $M_* = 1M_\odot$) are removed from the sample under the assumption they migrate all the way into their host stars without any stoppage. In relatively massive disks, early-generation embryos grow rapidly. Type I migration relocates these embryos from their birth place and delivers them to their host stars before they can attain isolation mass. Nevertheless, subsequent generations of embryos may form out of the residual planetesimals.

In order to simulate this continuous formation and migration sequence, we construct a prescription on the formation of next-generation seed embryos. When type I migration of any embryo formed at a_0 has led to the decay of its orbit to $0.5a_0$, we inject a new seed embryo at a_0 . In contrast to the initial mass (10^{20} g) for the first-generation seed embryos, the initial mass assigned to this born-again embryo is chosen to be 10^{-2} times that of its predecessor. If it is larger than the

¹ Recent Spitzer observations also support the bimodal population (Rebull et al. 2006; Cieza & Baliber 2007), while Corot observation may suggest single peak population, which means that this issue is still controversial.

isolation mass estimated from residual planetesimal surface density, the embryo mass is given by the isolation mass. (This prescription is introduced to merely represent the mass growth of residual planetesimals.) The growth rate and asymptotic mass of this embryo is determined by Σ_d of the local residual planetesimals. For example, its growth would cease if the total mass of planetesimals within its feeding zone is severely depleted. Detailed prescriptions on when to introduce any seed embryo and its assigned initial mass do not affect the final result.

In paper IV and V, we show that prior to severe gas depletion, this self-elimination process reduces Σ_d of the residual planetesimals and the asymptotic mass of late-generation embryos. During the gas depletion, a population of embryos is retained in the disk. Many of these late-generation embryos have sufficiently low masses to avoid extensive type I migration. In the absence of any magnetospheric cavity, since all the early-generation embryos are lost to their host stars, the mass and spatial distributions of the asymptotically-retained embryos are not sensitive to the initial magnitude of Σ_d . In the inner disk regions where growth time scale of embryos at their isolation masses is shorter than their migration time scale, they accrete all the planetesimals in their feeding zone. After gas depletion, the retained embryos continue to perturb each other’s orbits until they undergo orbit crossing and collide with each other (see §2.6). In the outer disk region, embryos are embedded in residual planetesimals in their feeding zones. Through dynamical friction, these planetesimals damp embryos’ eccentricities even after the disk gas is completely cleared away (? , also see §3.2).

Around strongly magnetized host stars, surface density of the gas Σ_g vanishes at $r < r_m$, where r_m is the radius of the outer boundary of the magnetospheric cavity. Outside this cavity, Σ_g reaches a local maximum at $r = r_{max}$. In the zone at $r_m < r < r_{max}$, pressure gradient in the disk tends to be positive and angular momentum is transferred from the disk to the isolated embryos through their unsaturated corotation resonances. Nevertheless, embryos may also lost angular momentum to the disk through their Lindblad resonances (Tanaka et al. 2002; Tanaka & Ward 2004). Embryos migration is quenched when they attain an torque equilibrium (Masset et al. 2006, Paper V).

When a pair of resonant embryos migrate to the inner disk edge, they experience a much stronger positive torque than that on a single embryo (Ogihara et al. 2010). As we indicated above, resonant embryos’ eccentricities are excited due to the conservation of an adiabatic invariance. Asymmetric eccentricity damping near the inner disk boundary leads to a net flow of angular momentum from the disk to the embryos. In the linear calculations (Tanaka et al. 2002; Tanaka & Ward 2004) the timescale of the eccentric damping (τ_e) is shorter than that of type I migration (τ_{mig}) by a factor of $\sim (c_s/v_K)^2 \sim O(10^{-3})$. (In this paper, we consider relatively slow migration with $C_1 \sim 0.1$ so that τ_e/τ_{mig} is expected to be even smaller.) Thus, angular momentum replenishment to the innermost resonant embryo is sufficient to compensate for the loss of it due to type I migration torques on all the trapped resonant embryos. Through a series of N-body simulations which include the damping due to disk-embryo interactions, Ogihara & Ida (2009) confirmed that this “eccentricity trap” can indeed stall the migration of a convoy of resonant planets. Based on these results, we consider a limiting case in which the innermost embryos are halted beyond the

edge of the cavity.

In the next section, we only present models in which type I migration is stalled at the outer boundary of the magnetospheric cavity. Nevertheless, we consider an alternative prescription in which we neglect the effect of eccentricity trap at the edge of the magnetospheric cavity. In that case, innermost embryos are often forced into the cavity by the torque from outer embryos. Models generated with this prescription predict a large population of very short-period planets which do not seem to be consistent with the findings of recent radial velocity surveys.

For computational convenience, we set the edge of the magnetospheric cavity at 0.04 AU. In reality, the location of inner edge depends on the stellar magnetic field and gas accretion rate which evolve during the disk depletion. We will consider these evolutionary effects in the next paper.

2.6. Post-oligarchic growth after gas depletion.

In Papers I-V, we used Equation (5) to compute embryos’ planetesimal-accretion rate. This formula was accurate for the population synthesis of gas giant planets because we need to determine the formation and retention of sufficiently massive cores in gas-rich environments (so that these cores can accrete gas and evolve into gas giants). In such an environment, cores’ eccentricity is suppressed and they attain isolation masses rather than engage in giant impacts.

Although their building-block embryos may have also formed in gas-rich disks, rocky/icy planets’ final assemblage need not proceed prior to the gas removal. In typical protostellar disks, embryos’ eccentricity is effectively damped so that their growth is limited by dynamical isolation. However, on the time scale of $\tau_{\text{dep}} \sim$ a few Myr, gas in these disks is depleted by viscous diffusion or photoevaporation while residual planetesimals are exhausted by embryos’ accretion except in outer regions. With a decline in embryos’ eccentricity damping efficiency, their orbits become dynamically unstable on time scales which increase with both embryos’ separation and Σ_g (Chambers et al. 1996; Zhou et al. 2007). Embryos’ eccentricities increase until their orbits cross (on a crossing time scale τ_{cross}) and their growth resumes through giant impacts. At the end of this post-oligarchic growth, the masses of the largest embryos typically increase by a factor of several to 30 (e.g., Kokubo et al. 2006). Thus, giant impacts essentially determine the asymptotic properties of rocky/icy planets.

Although we have not considered the dynamical interaction between multiple embryos in Papers I-V, an effort was made to approximate the outcome of giant impacts. In our previous prescription, the possibility of mergers after the gas depletion was simulated with the expansion of embryos’ feeding zone. In the construction of mass distribution for close-in rocky/icy planets (Paper V), we also considered two extreme limits, *i.e.* either all or none of the embryos migrated to the stellar proximity merge.

In order to accomplish the task to simulate the mass, semimajor axis, and eccentricity distributions of multiple super-Earths/Earths systems, we need to construct a prescription which

approximates the process of embryos’ eccentricity excitation and collisions through giant impacts. Our previous application of Equation (5) to the determination of mass growth associated with these giant impacts are not accurate. Here, we construct, in the Appendix, an improved prescriptions for embryos’ eccentricity growth in gas free environment and giant impacts. We outline below our computational procedures in a sequential order.

- 1) We compile a list of both dynamically isolated embryos and orbit-crossing pairs. We evaluate the time scale (τ_{cross} , see Appendix) for all dynamically isolated embryos’ eccentricity to grow until they cross the orbits of their closest neighbors.
- 2) We identify the pair of non-orbit-crossing embryos with the shortest τ_{cross} .
- 3) After such a time interval has elapsed, we compute the expected statistical changes in their eccentricity and semimajor axis. We then identify all other embryos whose orbits this pair would cross if these changes were implemented.
- 4) For this group of two or more embryos, we implement statistical changes in e and a due to repeated close scattering among themselves.
- 5) We apply corrections on the magnitude of semimajor axis changes among the participating embryos in order to preserve the conservation of total orbital energy.
- 6) We identify pairs of impacting embryos based on their statistically weighted collisional probability.
- 7) Under the assumption that these events lead to cohesion, we adjust both a and e of the merger product to satisfy the conservation of orbital angular momentum.

The search for potentially orbit-crossing pairs (step 2) are also applied to resonant embryos. In this context, Terquem & Papaloizou (2007) and Ogihara & Ida (2009) found through N-body simulations that, for rapid migration (with $C_1 = 1$), several embryos remain locked in mutual mean motion resonances near the disk inner edge after gas depletion and dynamical relaxation. These results indicate that multiple resonant configuration with relatively small number of bodies is stable and the formula for τ_{cross} (eq. [15]) cannot be accurately applied to such configuration.

However, Ogihara & Ida (2009) also found that for migration with $C_1 \ll 0.1$, resonant capture is more effective and produce convoys of several (up to dozens) resonant embryos over wide regions of the disk ranging from its inner edge to radii beyond 0.1AU. Resonant configuration of these resonant convoys is dynamically unstable and they always start orbit crossing and merge with each other after disk gas depletion. Since we are concerned with the relatively slow migration ($C_1 < 1$) in this paper, we adopt eq. (15) for τ_{cross} even for the resonance-trapped bodies.

The above procedure is repeatedly applied while the number of residual embryos declines and their separation increases with time. Eventually, the magnitude of τ_{cross} for all residual bodies exceeds a Gyr age of their host stars. We classify these asymptotic kinematic properties as dynamical architecture of mature systems. Although these comprehensive procedures are complicated

to integrate, each step is based on well-studied celestial mechanics. Other than two empirical parameters, there is no need to introduce any arbitrary assumptions. The two parameters are also qualitatively inferred from celestial mechanics (see Appendix), albeit their quantitative values are calibrated by N-body simulations by Kokubo et al. (2006). Thus, this semi-analytic scheme minimizes uncertainties in the embryos’ dynamical evolution.

2.7. Comparisons between the semi-analytic and N-body simulations

In order to assess the validity of our semi-analytic scheme, we make direct comparisons with the results of analogous N-body simulations. Kokubo et al. (2006) have performed N-body simulations for the giant-impact stage from isolated embryos to terrestrial planets. They systematically varied the initial disk mass, or equivalently the isolation mass and number of embryos in the radial range of 0.5-1.5AU. Since they carried out 20 runs with different initial azimuthal distribution of the embryos for each disk mass, the results of these simulations statistically represent asymptotic state of these systems.

With our prescription, we simulate the evolution of embryos systems with similar sets of initial masses and radial distributions. Figures 1 show a typical example of embryos’ post-oligarchic evolution. In this model, we consider systems which initially contain 16 embryos with $M_p \sim 0.1\text{--}0.2M_\oplus$. These embryos represent oligarchics which have attained isolation masses in a MMSN-type disk (*i.e.*, with $f_{d,0} = 1$). The thick and thin lines in the lower panel of Figures 1 correspond to the semimajor axes and peri/apo-centers of the embryos’ orbits. Close scatterings lead to embryos’ eccentricity excitation and semimajor axis diffusion. Line discontinuities represent merger events between nearby embryos. The upper panel shows semimajor axes and eccentricities of planets in an asymptotic state. All planets are assumed to have identical internal density and the radii of their representative circles are scaled to be proportional to their physical radii. In this model, four planets with masses $0.11M_\oplus$, $0.44M_\oplus$, $1.0M_\oplus$, and $0.76M_\oplus$ survive in stable orbits at 0.46AU, 0.56AU, 0.85AU, and 1.74AU, respectively.

In order to consider the statistical properties of these embryos systems, we also simulated a set of 20 runs for the same initial f_d with our numerical prescription, analogous to the previous direct N-body simulations. Figures 2 show the averaged mass, semimajor axis, and eccentricity of the most massive bodies and their standard deviations in their final state. For comparisons, these figures include the results obtained by N-body simulations of Kokubo et al. (2006) and our semi-analytical model (panels a and b). We also plotted the same quantities for the second most massive bodies in panels c and d.

The results plotted in these figures include sets of initial conditions with $f_d = 0.3, 1$ and 3 . Embryos’ initial masses are given by their isolation masses and initial semimajor axes are distributed from 0.55AU to 1.5AU with orbital separations of $10r_H$. The total mass of the distributed embryos is $0.72M_\oplus$, $2.3M_\oplus$, and $6.66M_\oplus$ for $f_d = 0.3, 1$, and 3 , respectively. According to the values of

f_d , number and masses of initial embryos are changed. We used the same initial conditions as Kokubo et al. (2006) (see their Table 1).

The figures show very good agreement in planets’ asymptotic mass and semimajor axis between the N-body simulations and our models for all initial conditions. The dependence of planets’ asymptotic mass on f_d is well reproduced. Although there is a difference in the expectation value for e of the second most massive bodies, it is within a standard deviation. Note that our model runs several orders of magnitude faster than the direct N-body simulations, so we can incorporate the post-oligarchic dynamical interactions into our synthetic planet formation simulations.

2.8. Transition from marginal metastability to protracted order

After the embryos’ eccentricity is excited to the magnitude which enables them to cross other’s orbit, their close encounters lead to either elastic scattering or mergers. (For these self-gravitating embryos, we neglect the effect of fragmentation and differentiation between volatile and refractory materials.) Repeated elastic scattering further increases embryos’ eccentricity to a value e_{esc} which is the ratio of embryos’ surface escape velocity and their Keplerian velocity (see Appendix). With this eccentricity, the Safronov number is of the order unity and gravitational focusing no longer dominates the collisional cross section.

Orbit crossing events can also lead to direct collisions and merger events. These cohesive collisions reduce the number of surviving planets and widen the separation between them. Although some merged embryos’ orbits may become temporarily isolated, dynamical instability can re-excite their eccentricity. If this marginally stable state can be maintained, the number of surviving massive embryos would continue to decline while τ_{cross} would become comparable to the age of the system.

However, as we discuss in Appendix, e of the merged embryos are often significantly smaller than those of their progenitors prior to the collision. These merger events generally involve embryos with limited range of relative longitude of periastrons centered around 180 degrees. For Keplerian motion with $e \ll 1$, the mass-weighted total Laplace-Runge-Lenz (LRL) vector is conserved (Nakazawa & Ida 1988, 1989). Mergers of embryos with anti parallel longitudes of periastron generally lead to fractional cancellation in the mass-weighted total LRL and therefore relatively small values of e of the merged embryos (for details, see Appendix). Consequently, the asymptotic e of the surviving embryos is generally smaller than e_{esc} . This efficient damping is consistent with the results of previous N-body simulations (Kokubo et al. 2006).

With this efficient damping process, many merged embryos’ orbits become temporarily isolated. Although dynamical instability can re-excite their eccentricity, the crossing time (τ_{cross}) given by eq. (15) often abruptly increases after some merger events. Figures 3 show time evolution of the maximum planetary mass (M_{max}) (the top panel), total number (the middle panel) and the minimum crossing time (the bottom panel) in five independent runs of our semi-analytical models with $f_d = 1$ and initial number of the embryos $n = 16$. After n decreases to 3–4 and M_{max} grows

to $\sim M_{\oplus}$, τ_{cross} abruptly jumps from $\tau_{\text{cross}} \lesssim 10^6$ yrs to $\tau_{\text{cross}} \gtrsim 10^{10}$ yrs, so the systems make a transition to a dynamically stable state, on Gyr main-sequence life-span of solar-type stars. Since these changes in the mass and eccentricity growth rates are comparable to the gas depletion time scale in the disk, stochastic merger events can introduce diversity in the extent of type I migration of the surviving embryos.

3. Population Synthesis of Planetary Systems

With this new scheme, we simulate the formation of rocky and icy planets. The predicted mass, size, period, and eccentricity distribution of close-in Earths/super-Earths that can be used to directly compare with observational data (Schlaufman et al. 2010).

3.1. Initial conditions

In Papers I-V, we presented a series of simulated planetary mass-semimajor axis distributions. We adopt a range of disk model parameters which represent the observed distribution of disk properties and assign them to each model with an appropriate statistical weight. (For example, more massive ($f_g > 1$) and long lasting ($\tau_{\text{dep}} > 3 \times 10^6$ yrs) disks are adopted less often than low-mass disks.) For each disk, although several planets may be generated over time, their mass growth and orbital evolution are treated independently. (Evolution of the Σ_d distribution was simulated with a simplified prescription, see §2.2). Mergers and giant impacts after gas depletion are approximated by planetesimal-accretion formula for disks’ outer regions and artificially enforced (or neglected) in the stellar proximity. In Papers I-V, embryos’ dynamical interaction with each other is neglected in our population synthesis models, and planets’ asymptotic mass and period distributions are obtained from the compilation of many monte carlo simulations. These properties only represent systems which contain single planets, regardless of their masses.

Solar System contains four terrestrial planets, two gas giants and two ice giants. Many extrasolar planets have known siblings. Perhaps, all planets reside in multiple-planet systems, albeit many members may have sufficiently low mass to be below the detection limit. Nevertheless, their dynamical interaction may affect the overall kinematic structure of planetary systems. Even in systems which contain only one massive gas giant, its dynamical influence on other residual embryos may affect their asymptotic architecture.

In this and subsequent papers, we will use our modified prescriptions described in the last section to generate statistically-weighted mass-period distributions for multiple-planet systems. Since there are many competing dynamical processes which may affect the outcome of these simulations, we adopt a step-by-step approach with increasing degrees of complexity. Here we first carry out some case studies. In these preliminary models, we only consider systems around G dwarfs with solar mass and metallicity. (Stellar mass and metallicity dependences will be considered in future

investigations.) We focus in this paper on the formation of rocky/icy planets in the absence of any gas giants and only consider disks with modest masses (with initial $0.3 \leq f_d = f_g \leq 3$). For these low-mass systems, planets’ weak secular perturbation on each other has been taken into account in our treatment of post-oligarchic growth. (In addition to nonlinear close-encounters, gas giants, if present, can also induce sweeping secular and resonant perturbations which will also be considered in future papers.)

The initial distributions of Σ_d and seed planetesimals are specified in §2.2. We introduce some small random fluctuations to the initial locations of the seed planets for different runs. Mass growth and orbital evolution of embryos are computed with the prescriptions in §2.2–§2.5. We do not consider the possibility of giant impacts among embryos in a gas-rich environment because these events must be preceded by embryos’ orbit crossing (§2.6). Iwasaki et al. (2002) and Kominami & Ida (2002) showed that orbital crossing can occur only after Σ_g is sufficiently depleted so that gas can no longer suppress embryos’ eccentricity excitation. Here, we adopt a necessary condition for orbit crossing to be $f_g/f_{g,0} < 10^{-3}$. Since we use $f_g = f_{g,0} \exp(-t/\tau_{\text{dep}})$ with $\tau_{\text{dep}} = 3 \times 10^6$ yrs, orbit crossing is possible at $t > 2 \times 10^7$ yrs.

Dynamical friction from a planetesimal swarm can also suppress orbit crossing. We calculate the total planetesimal masses in the feeding zones of embryos at each timestep. If the total mass in their feed zones is larger than any embryos’ mass, we suppress their orbit crossing. (These embryos are not included in the orbit crossing bodies in step 4 in the procedures described in Appendix §2.6). Since their growth is slow in outer regions, embryos’ perturbation on each other is limited and they do not undergo orbit crossing in the absence of any gas giants. We assign an eccentricity $\sim r_{\text{H}}/a$ to each embryo which does not undergo orbit crossing (see step 1 in Appendix).

3.2. Overall evolution with dynamical interactions

We first consider a disk with a modest initial mass ($f_{d,0} = 2$) and migration efficiency $C_1 = 0.1$. For illustrative purpose, only seed embryos at 0.5–15AU are integrated in this particular model. We apply two different sets of inner boundary conditions: 1) embryos’ migration is stalled by a cavity (see Figures 4) or 2) they are not stalled at all. (In subsequent papers, we will consider the possibility that some embryos may be forced to undergo further inward migration by the perturbation of additional embryos which migrated to their outer low-order main-motion resonances.) The bottom panels of these two figures show the time evolution of semimajor axes of all embryos and the top and middle panels show eccentricities and masses of final planets at $t = 10^9$ yrs.

In inner regions, embryo growth due to planetesimal accretion and migration are so fast that multiple-generation embryos are formed. In the bottom panels, the lines starting at 10^5 – 10^7 yrs represent 2nd/3rd-generation embryos. Due to their smaller masses, type I migration of 2nd/3rd-generation embryos is relatively slow. They are usually captured and shepherded by the mean-motion resonance of 1st-generation embryos that have migrated in from outer regions.

At $t > 2 \times 10^7$ yrs, gas is sufficiently depleted that it can no longer effectively damp embryos' eccentricity. Thereafter, orbit crossing and coagulations between embryos occur on timescales of 10^7 – 10^8 yrs. In outer regions, embryos grow slowly and they do not migrate over significant distances. Due to dynamical friction by a large population of residual planetesimals, these embryos do not start orbit crossing even at $t > 2 \times 10^7$ yrs.

In the model with a magnetospheric cavity (Fig. 4), a convoy of migrating embryos (formed interior to $a \sim 4\text{AU}$) congregate and park near the disk edge. Their total mass is $\sim 20M_{\oplus}$. These embryos are captured into the mean-motion resonances of embryos which have arrived in the stellar proximity at earlier times. This group of resonant embryos extend from the inner edge of the disk to radii beyond 0.1AU. (This phenomenon is observed in the N-body simulation by Ogihara & Ida (2009) in their slow migration case.) After disk gas depletion, eccentricity excitation by embryos interaction with each other is no longer damped by their tidal interaction with the disk. As their eccentricity grows, embryos cross each other's orbit. Close encounters break up their mean motion resonance and this group of embryos collide with each other to form six planets with mass in the range of $\sim 1 - 10M_{\oplus}$ between 0.03 and 0.5 AU. In the absence of any residual gas, they cannot migrate into resonance again.

Figure 6 shows the time evolution of the scaling factor (f_d) for planetesimal surface density due to accretion by embryos in the case of the result in Figure 4. In Paper IV, we analytically derived the radius beyond which this surface density is nearly preserved to be $a_{\text{dep,mig}} \sim C_1^{1/8} (t/10^6 \text{yrs})^{1/4}$ yrs. That analytical formula agrees with the numerical result presented here. In outer regions, embryos start their migration when their masses are much smaller than their isolation masses, so the depletion in f_d there is small. These residual planetesimals provide damping of embryos' eccentricities and thereby suppress orbit crossing and giant impacts in their post-oligarchic stage. However, in inner regions ($\lesssim 1\text{AU}$), most of planetesimals have been accreted by 1 Myr. This clearing enables the post-oligarchic growth through orbit crossing and coagulations between isolated embryos after gas depletion.

We also consider a model without any migration barrier at the edge of the magnetospheric cavity (see Fig. 5). In this case, many first generation embryos migrate into their host stars. No close-in ($\lesssim 0.1\text{AU}$) Earths/super-Earths survives. Two super-Earths with $0.8M_{\oplus}$ and $7M_{\oplus}$ emerge at 0.18 AU and 0.4 AU respectively.

3.3. Planetary growth in the inner and outer disk regions

For a solar composition, the critical core mass to hydrodynamically sustain gas envelope is $M_{\text{c,hydro}} \sim 10M_{\oplus}$ (Mizuno 1980; Pollack et al. 1996; Ikoma et al. 2000). Its magnitude also depends on the planetesimal accretion rate, atmospheric composition (Ikoma et al. 2000) and the boundary condition between protoplanets' atmosphere and their natal disk (Ikoma et al. 2001). In the stellar proximity where the disk gas is relatively dense and hot, magnitude of $M_{\text{c,hydro}}$ may be smaller

(Ikoma et al. 2001). Once the core mass (M_c) exceeds $M_{c,\text{hydro}}$, envelope starts contracting. If $M_c > M_{c,\text{crit}} \sim \text{several}M_\oplus$, the contraction timescale may be less than disk lifetime (Paper I), although $M_{c,\text{crit}}$ also depends on atmospheric composition. If embryos arrive in the stellar proximity with $M_p \gg M_\oplus$, they may initiate rapid phase of gas accretion and evolve into hot Jupiters (Bodenheimer et al. 2000).

However, embryos’ growth in inner regions is regulated by their type I migration and characterized by a two-stage growth (runaway/oligarchic growth and post-oligarchic growth) process. Prior to gas depletion, embryos with mass less than

$$M_{c,\text{max}} \simeq 0.21C_1^{-3/4} \left(\frac{f_{g,0}}{3}\right)^{3/10} \left(\frac{\eta_{\text{ice}}f_{d,0}}{f_{g,0}}\right)^{3/4} \left(\frac{a}{1\text{AU}}\right)^{-9/8} \left(\frac{M_*}{M_\odot}\right)^{5/4} M_\oplus \quad (13)$$

grow *in situ*, i.e., they gain mass faster than they undergo type I migration. (The critical mass for resistance against type I migration $M_{c,\text{max}}$ is determined by the condition $\tau_{\text{mig1}} = 3\tau_{c,\text{acc}}$, where a factor 3 reflects an actual timescale to reach M_c because $\tau_{c,\text{acc}} \propto M_c^{1/3}$.) In regions of disks where embryos can attain $M_{c,\text{max}}$ before they acquire all the residual planetesimals within their feeding zone would migrate to and accumulate near the disk inner edge. Prior to disk gas depletion, since these embryos cannot undergo orbit crossing, their growth through cohesive collisions are temporarily quenched.

Despite being surrounded by gas, these stranded embryos cannot evolve into gas giants in disks with modest $f_{d,0} (< 10)$ because the magnitude of $M_{c,\text{max}}$ is well below the critical core mass ($M_{c,\text{crit}}$) for the onset of efficient gas accretion. Close-in embryos do significantly increase their masses through giant impacts to magnitude $> M_{c,\text{crit}}$ after the disk gas depletion, especially in disks with $f_{d,0} \gtrsim 2 - 3$. But, there would be little residual gas for these embryos to accrete and they are likely to evolve into super-Earths rather than the cores of gas giants. Through this process, close-in super-Earths may bypass their isolation masses without becoming gas giants. Thus the detection of relatively massive compact planets (with $M_p > 10M_\oplus$) does not necessarily imply a high magnitude for $M_{c,\text{crit}}$.

In the outer regions, on the other hand, planetary growth ends in runaway/oligarchic growth stage and type I migration is much less effective. Since isolation mass increases with a , embryos emerge outside the ice line can acquire $M_p > M_{c,\text{core}}$ and evolve into the cores of gas giants before gas depletion (Paper I). As we stated in the introduction, this paper focus on the low-mass disks which do not produce gas giants. In fact, in our disk models with $f_d = 2$, embryos with a few M_\oplus emerge at $a \sim 3\text{--}5\text{AU}$ (see Figs. 4 and 5). In the next paper, we will consider dynamical perturbation induced on the residual embryos by one or more emerging gas giants (we will also take into account the effect of an ice-line barrier in more massive disks, see Paper V). We anticipate a large fraction of residual long-period planetesimals and embryos may be ejected as they are scattered by one or more gas giants.

3.4. Assemblage of rocky planets after gas depletion.

In this section, we consider the detailed evolution of rocky/icy planets after gas depletion. Using the prescription presented above, we present planets’ asymptotic $M_p - a$ and $e - a$ distributions for several sets of simulations with a range of magnitude in C_1 and $f_{d,0}$. Seed embryos are initially distributed between 0.2–20AU (see §3.1). Dynamical interaction between multiple embryos is a stochastic process which would be inadequately represented by the results of any single set of simulations. In order to characterize planets’ statistical distribution for each set of model parameters, 20 totally independent series of random numbers are used to compute their progenitors’ dynamical interaction. From these Monte Carlo simulations, we obtain the mean values of M_p , a , and e as well as their standard deviations. In this analysis, computation with our semi-analytical prescription is much faster (by several orders of magnitude) than direct N-body simulations.

The asymptotic (at $t = 1\text{Gyr}$) $M_p - a$ (left panels) and $e - a$ (right panels) distributions for models with $f_{d,0} = 3$ and $C_1 = 0, 0.03$, and 0.3 are shown in the top, middle, and bottom panels of Figures 7. In these models, we consider highly magnetized host stars and impose a magnetic cavity in the disk and assume embryos’ type I migration is stalled there (see §2.5). In §3.5, we consider the possibility of negligible stellar magnetic field.

For presentation purpose, we divide the emerging embryos into the close-in ($a < 0.1a_{\text{ice}}$), inner ($0.1a_{\text{ice}} < a < 0.3a_{\text{ice}}$), outer terrestrial ($0.3a_{\text{ice}} < a < a_{\text{ice}}$), and icy ($a_{\text{ice}} < a$) planet regions. We record number of planets in each region, asymptotic (at $t = 1\text{Gyr}$) mass, semimajor axis, and eccentricity of planets in order of mass in each region. The quantities are averaged over the most massive planets, the second most massive planets, the third most massive planets, ... in each region. In Figures 7, we plot planets of the averaged number in each region.

The results in Figures 7 show that typically three terrestrial (rocky) planets emerge in the $C_1 = 0$ (no type I migration) model. Since these planets contain all the building blocks interior to the ice line, they have masses of a few M_{\oplus} . (In comparison, for the idealized model in Figure 2, lower-mass planets emerge from planetesimals which were initially located within 1.5 AU in a MMSN.) These planets attain relatively small orbital eccentricities (~ 0.1). Their corresponding velocity is considerably smaller than their surface escape velocity. In §2.2 and Appendix, we suggest that merger events generally lead to some degree of energy dissipation. Nevertheless planets’ asymptotic eccentricities are larger than current eccentricities of Venus and Earth. Dynamical friction from residual disk gas (Kominami & Ida 2002) or residual planetesimals (O’Brien et al. 2006) may further damp the eccentricities. Because we keep track the amount of residual disk gas and planetesimals, these effects can be accounted for in subsequent papers.

According to equation (13), Earth-mass rocky embryos can relocate from all radii interior to the ice line to the proximity of their host stars prior to the gas depletion even with inefficient type I migration. For models with $C_1 = 0.03$, dozens of embryos form interior to the ice line with masses $\sim M_{c,\text{max}} \sim 0.2M_{\oplus}$ and then migrate to the vicinity of their host star. After gas depletion, these embryos undergo dynamical relaxation and cohesive collision to assemble into several super-Earths

with $a \lesssim 0.3$ AU. Similar results are produced in models with $C_1 = 0.3$ (see middle and lower panels of Figures 7). Although more efficient type I migration depletes the residual planet-building blocks at several AU, the asymptotic planet distribution close to their host stars is not very different between models with $C_1 = 0.03$ and $C_1 = 0.3$. In both models, all the migrated embryos are halted near the inner edge. Post depletion giant impacts lead to the assemblage of similar mass super-Earths, albeit the number of close-in super-Earths appears to increase with C_1 .

Simulation results for models with less massive disks are shown in Figures 8 ($f_{d,0} = f_{g,0} = 1$) and 9 ($f_{d,0} = f_{g,0} = 0.3$). Equation (13) shows that in disks with similar metallicity ($f_{d,0}/f_{g,0}$), $M_{c,\max}$ increases with $f_{g,0}$. In principle, small embryos can participate in type I migration. But, embryos' growth is also limited by dynamical isolation. Equation (6) indicates that the magnitude of the isolation mass $M_{c,\text{iso}}$ also increases with $f_{d,0}^{3/2}$. In disk regions where $M_{c,\text{iso}} < M_{c,\max}$, many embryos emerge without type I migration. In addition, Equation (8) indicates that the embryos' migration timescale decreases with both their masses and f_g . In the limit of inefficient ($C_1 = 0.03$) or no ($C_1 = 0$) migration, embryos would not migrate over significant distance if their $\tau_{\text{mig1}} > \tau_{\text{dep}}$. Limited migration reduces the delivery of building block material to the stellar proximity. Consequently, the probability of forming short-period super-Earths is an increasing function of $f_{d,0}$. (The emergence of short-period Earth-mass planets from modest to low-mass disks requires relatively efficient type I migration with $C_1 > 0.3$).

In contrast, the retention of embryos near their cradles (just interior to the ice line) promotes the formation of rocky planets with intermediate periods (months to years). After gas depletion, post-oligarchic growth continues through giant impacts on a time scale which is an increasing function of a . In a MMSN-like disk (with $f_{d,0} = 1$), a system 4-5 planets emerge (on time scale of ~ 100 Myr) with comparable masses, semimajor axes, and slightly larger eccentricities to those of the terrestrial planets in the solar system. Due to the difference in the impact of type I migration, the formation probability of potentially habitable planets in this model is actually higher than that out of more massive ($f_{d,0} = 3$) disks (see Figures 7).

3.5. Formation of super-Earths around protostars with weak magnetic fields

In the limit of negligible stellar magnetic field, protostellar disks extend to the stellar surface (see §2.5). In the absence of a magnetospheric cavity, migrating embryos are unable to be halted. The importance of this inner boundary condition is highlighted in Figures 10 which represent models with the same value of $f_{d,0}(= 3)$ as the model in Figures 7. (In this series of simulations, the onset of efficient gas accretion is artificially suppressed. In a subsequent paper, we will consider the concurrent formation of gas giants and super-Earths.)

With modest migration efficiencies ($C_1 = 0.03$ and 0.3), embryos formed within $\sim 1 - 2$ AU prior to gas depletion attain mass $\sim M_{c,\max}$ and migrate all the way into their host stars. They either accrete residual planetesimals or capture other embryos along their migration paths and clear

the inner ($\lesssim 1$ AU) region around their host stars. At $a \gtrsim 2$ AU, embryos’ migration is initiated before they reach their isolation masses (see Paper IV). After the gas depletion, multi-generation embryos with non-negligible masses are retained. These embryos undergo orbit crossing as their eccentricity is excited by their mutual perturbations. Through post-gas-depletion giant impacts, they merge into Earth-mass planets. Beyond the ice line, cores at 4–5 AU have masses of $\sim 10M_{\oplus}$. But, these systems do not contain any Earth-mass planets with periods less than a few month. This asymptotic dynamical architecture (*i.e.*, $M_p - a$ distribution) is similar to that of the Solar System.

3.6. Production of debris disks

Observationally, there is no clear correlation between the detection of gas giant planets and that of debris disks around common host stars. While the fraction of solar type stars with known gas giants increases with their metallicity (e.g., Fischer & Valenti 2005, also see Paper II), there is no analogous correlation between stellar metallicity and the presence of debris disks around them (Greaves et al. 2007).

Debris disks are composed of grains with sizes comparable to the infrared wavelengths (a few μm to sub-millimeter). Around mature solar stars, smallest (sub-micron) grains are blown out by radiation pressure. Due to Poynting-Robertson drag, modest (sub-mm) grains undergo orbital decay on time scale (a few Myr) shorter than the age of their host stars (e.g., Takeuchi & Artymowicz 2001). Thus, these grains must be continually generated through collisions of their parent bodies.

In all the models we have considered here (regardless the magnitude of C_1), embryos growth prior to gas depletion is limited by dynamical isolation in the inner disk regions. After gas depletion, post-oligarchic giant impacts inevitably occur, regardless of the stellar metallicity. Thus, the production of “warm” debris dust (with wavelength up to $\sim 10\mu\text{m}$) is expected to be common around all solar type stars.

If, in the inner disk region, a large fraction of the total mass in heavy elements is attained by the largest embryos, time scale generating a large pool of warm debris particles (τ_{cross}) would be longer than the grains’ clearing time scale but shorter than the age of mature host stars (Gyr). Thus, replenishment of detectable grains in debris disks may be a stochastic process and the intensity of debris disk signature may vary episodically (Kenyon & Bromley 2004).

In outer disk regions, planetesimal growth is incomplete with a large amount of residual planetesimals (see §3.2). Embryos’ eccentricities in this region are likely to be excited by close encounters or merger events with other embryos and damped by gas through tidal interaction and residual planetesimals through dynamical friction. Unless icy embryos become sufficiently massive to efficiently accretion gas (more massive than $M_{c,\text{crit}}$), their surface escape velocity ($\sim 10 \text{ km s}^{-1}$) is generally smaller than Keplerian velocity at $a < 10$ AU. Consequently, close-encounters with embryos do not lead to the ejection of residual planetesimals. In this limit, planetesimals’ velocity

dispersion is excited by embryos’ repeated gravitational perturbation and damped by inelastic collisions among themselves. When an equilibrium is established, planetesimals’ velocity dispersion becomes comparable to the surface escape speed of the planetesimal population which carries most of the masses.

If these planetesimals have sizes larger than a few km’s (as in the Kuiper Belt, (Pan & Sari 2005, e.g.), their velocity dispersion would exceed that for disruptive collisions (Stewart & Leinhardt 2009). Debris of such collisions would produce “cold” grains which reprocess stellar radiation and generate far infrared excess radiation (Wyatt 2008). Since the collision time scale for numerous km-size planetesimals is expected to be shorter than the grain depletion time scale, the signature of outer debris disk is expected to be maintained at a steady level.

In relatively massive disks where one or more embryos can attain critical mass for the onset of efficient gas accretion prior to the depletion of the disk gas, the formation of gas giants can scatter residual planetesimals to large distances. For example, in the Solar system, while residual planetesimals near Uranus and Neptune were scattered by them to the Kuiper Belt region or the Oort’s cloud, those in the vicinity of Jupiter and Saturn were either ejected or scattered to the distant Oort’s clouds (Duncan & Levison 1997). The clearing of residual planetesimals (as parent bodies) would suppress the signature of cold debris disks around stars with gas giants. Thus, around host stars with relatively low metallicity, the lack of gas giants does not necessarily imply a lower detection probability for debris disks.

3.7. Formation of close-in super-Earths

The results in previous sections indicate that a small amount of planet-disk tidal interaction can lead to significant type I migration for embryos more massive than $M_{c,max}$. In sufficiently massive disks (with $f_{d,0} > 1$), a convoy of embryos stall from outer edge of magnetospheric cavity (specified to be 0.04 AU in our models) to locations beyond 0.1 AU. (Around strongly magnetized stars or in less massive disks, embryos may be stalled at larger distances from their host stars). These embryos merge through giant impacts after gas depletion. Since only a fraction of embryos’ energy is dissipated, the resultant semi major axis of the merger products is expected to be comparable to that of their progenitor embryos.

Close encounters between embryos generally do not lead to mean motion resonance. In the absence of residual disk gas, these merger products do not undergo any further orbital decay and generally remain out of mean motion resonance with each other. These expectations are consistent with the simulated asymptotic $M_p - a$ distribution (see Figs. 7 and 8).

The velocity dispersion of the residual embryos is a fraction of their surface escape speed. In the stellar proximity, it is much smaller than the local Keplerian speed. In comparison with Earth-mass planets at around 1AU, the simulated eccentricities of close-in super-Earths are relatively small (in the range of 0.01–0.1). In subsequent papers, we will consider the possibility of excitation

of much larger eccentricity by secular resonances of distant gas giants (e.g., Mardling & Lin 2004; Nagasawa et al. 2005; Thommes et al. 2008b).

Many emerging planets have masses larger than $\sim M_{c,\text{crit}}$ which is the critical mass for cores to evolve into gas giants within a few Myr. Since these planets acquired most of their mass after the gas is depleted or in gas-free cavities, they cannot accrete a substantial gaseous envelope. The atmosphere of their progenitor embryos may also be ejected during giant impacts. Despite their challenges in attaining primary atmospheres, the emerged super-Earths may attain a metal-rich secondary atmosphere through outgassing. However, such an atmosphere would contribute to a small fraction of these planets’ total mass.

3.8. Frequency of habitable planets

In disks with Σ_g and Σ_d comparable to those of MMSN, embryos’ isolation mass at the habitable zone (~ 1 AU) is considerably smaller than that of the Earth. Nevertheless, terrestrial planets attain most of their asymptotic masses, after the gas depletion, through giant collisions and merger events as their velocity dispersion increases until they bypass their dynamical isolation. This conjecture is supported by the late Earth’s formation epoch ($\sim 30 - 60$ Myr as inferred from radioactive isotopes (e.g., Yin et al. 2002; Kleine et al. 2002)) which appears to persist well after the disk gas is depleted (on a few Myr time scale).

In Papers I-IV, this post-oligarchic growth has been taken into account with a simple prescription. In that approach, the width of embryos’ feeding zone ($\sim 2e_{\text{esc}}a$) is assumed to expand with their eccentricity and embryos’ asymptotic mass is estimated to be (Paper I)

$$M_{e,\text{iso}} \simeq 0.68 \eta_{\text{ice}}^{3/2} f_{\text{d}}^{3/2} \left(\frac{a}{1\text{AU}} \right)^{3/2} \left(\frac{\rho_{\text{d}}}{3\text{gcm}^{-3}} \right)^{1/4} M_{\oplus}. \quad (14)$$

This approximation naturally reproduces the dependences of the outcome on the magnitude of $f_{d,0}$ and a . In comparison the results simulated with our new prescription, the above expression for $M_{e,\text{iso}}$ slightly underestimates it (by a factor of ~ 2 or so).

Figure 4 in Paper V shows that a fraction of solar type stars harboring habitable planets with $M_p \simeq 0.3 - 10M_{\oplus}$ and $a \simeq 0.75 - 1.8\text{AU}$, $\eta_{\oplus} \sim 20\%$ for $C_1 \lesssim 0.03$ and $\sim 10\%$ for $C_1 \lesssim 0.3$. These values do not significantly change by using the present new model. Thus, with our new prescription, we verify that the magnitude of η_{\oplus} is adequately reproduced by the simulations presented in Paper V, using Eq. (14).

4. Summary and Discussions

In this paper, we introduce a new prescription for our population synthesis models. In this revision, we incorporate, for the first time, a semi analytic prescription for close scatterings and giant

impacts among solid planetary embryos (for detailed prescriptions, see Appendix). Our analytical model quantitatively reproduces statistics of the asymptotic distributions of mass, semimajor axis and orbital eccentricities of bona fide planets obtained by N-body simulations (Kokubo et al. 2006), as shown in §2.7.

We also take into account the effects of resonant trapping by embryos during their migration and when they are stalled by migration barriers (§2.4, 2.5). With these tools, we are able to simulate the statistical distributions of solid planets’ asymptotic mass, semimajor axis and orbital eccentricities, in systems without any giant planets.

These simulations are particularly relevant to the recently discovered population of close-in super-Earths. Our results indicate that the emergence of super-Earths in the proximity of their host stars proceeds through three stages:

- In a gas rich environment, embryos accrete planetesimals in their feeding zones and become dynamically isolated (runaway/oligarchic growth).
- Embryos undergo orbital decay and accumulate close to their host stars (migration/stall).
- After disk gas depletion, embryos perturb and excite eccentricities of each other. Eventually, their orbits cross and they grow significantly beyond the isolation mass through collisions among them (post-oligarchic giant impacts).

During the second and third stages, sub-Earth embryos evolve into systems of non-resonant, multiple super-Earth planets through the following mechanisms:

- The coupled effects of type I migration of embryos, termination of the migration near the inner disk edge, and resonant trapping between embryos produce a resonantly trapped convoy of embryos that extends beyond 0.1AU for the the cavity inner boundary condition (§3.2).
- In the presence of the disk gas, because their orbits are stabilized by efficient tidal e -damping, embryos’ individual masses are similar to the critical mass to resist against type I migration that is $\lesssim M_{\oplus}$. They do not go into runaway gas accretion phase.
- Through close scattering and giant impacts after disk gas depletion, the resonantly clustered embryos form multiple Earths or super-Earths in non-resonant orbits around ~ 0.1 AU in the disks with masses comparable to or a few times larger than the MMSN ($f_{d,0} \simeq 1-3$).
- Merger products attain non-resonant orbits and their orbit crossing timescale is longer than the typical age of their host stars (~ 10 Gyr). Consequently, their asymptotic dynamical architecture is very stable.
- Although the Earths/super-Earths suffer close scattering, their eccentricities are as low as 0.01–0.1 due to efficient collision damping and large local Keplerian velocity.

- Although the asymptotic mass of some super-Earths is larger than that required to initiate efficient gas accretion, they do not evolve into gas giants because their final assemblage occur only after the residual disk gas is depleted.

In disks with $f_{d,0} \lesssim 0.3$, the initial isolation mass of embryos interior to the ice line is considerably less than that of the Earth. Type I migration of sub-Earth embryos is less efficient and the amount of embryos accumulation in the stellar proximity is limited. Consequently, close-in planets, if formed at all, tend to have masses less than that of the Earth.

For a range of disk accretion rate (comparable to that observed in typical T Tauri stars), migration of embryos formed in the outer regions of protostellar disks is stalled by a barrier near the ice line (Kretke & Lin 2007, Paper V). Although the isolation mass at large distances from their host stars is substantially larger than that of the Earth, embryos’ growth time scale is also very long. Embryos may attain masses (mostly made of icy material) comparable to that of Uranus and Neptune but they would not be able to completely clear their feeding zone (even on a time scale of a few Gyr). Consequently, their eccentricity is effectively damped by dynamical friction from the residual planetesimals even after the disk gas is depleted.

In our simulations, we found a relatively large fraction of stars bear ice giants, albeit many of these stars do not contain any gas giants. While ice giants tend not to cross each other’s orbits, they, nonetheless, scatter residual planetesimals to large distances (beyond 10-100 AU’s, analogous to the Kuiper Belt) and continuously supply parent bodies of debris disks which emit persistent (over Gyr time scale) mid and far IR reprocessed radiation (equivalent to cold zodiacal light). In the region interior to the ice line, embryos’ growth is suppressed by dynamical isolation rather than collisional time scales and a few super-Earth oligarchics emerge while residual planetesimals between them are mostly acquired by them. In this region, post-oligarchic collisions occur stochastically and produce dusty fragments which provide sources for the NIR reprocessed radiation (Kenyon & Bromley 2004). The occurrence of inner debris disks only weakly depends on the host stars’ metallicity and mass through the asymptotic mass and spacing of the embryos.

The cases presented here are for disks with modest mass. In relatively massive ($f_{d,0} \lesssim 2 - 3$) or metal-rich disks, one or more gas giants may form (Paper I, IV). We have not considered here systems which contain gas giants. The effects of their secular and resonant perturbation will be considered in the next paper. Here we draw to the attention that our Solar System does not have any planetary body inside Mercury’s orbit at 0.4AU. Yet it must have formed from a disk with $f_{d,0}$ comparable to or larger than unity (*i.e.*, at least in a MMSN). Many extrasolar planetary systems also do not display any sign of close-in super-Earths. We suggest this dichotomy is due to a dispersion in the sizes of an inner disk cavity. The extent of this disk region depends on the diverse disk accretion rate and strength of host stars’ magnetic field during their T Tauri phase of evolution.

In §2.5, we suggested that the observed bimodal distribution of spin periods of young stars with peaks at about one week and one day respectively may be produced by the different strength

of the coupling (Herbst & Mundt 2005). If the coupling is stronger than some critical value (around stars with a few kilogauss fields), the stellar spin angular momentum would be transferred to the disk through the stellar dipole magnetic field and the ionized disk gas would be accreted through the channel flow along the magnetic field lines (e.g., Shu et al. 1994). Inside the radius ($\sim 0.06\text{--}0.1$ AU) where disk gas and stellar spin co-rotate (with period of a week), the disk would lose angular momentum and be truncated with a magnetospheric cavity (e.g., Shu et al. 1994).

This magnetospheric cavity may not exist or be confined to much smaller radii around stars with relatively weak magnetic fields. Inefficiency of angular momentum transfer would result in much faster stellar spin (with periods of a day). In this limit, migrating embryos would be halted (if at all) so close to their host stars that the star-planet tidal interaction would lead to further orbital decay and disruption. We simulated such a possibility with models in which no migration barrier is imposed at the disk inner boundary (see §3.2 and 3.4). We find that regions interior to ~ 0.3 are effectively cleared by early generation of migrating embryos.

First-generation embryos may have formed in the primordial solar nebula when the infant Sun had a relatively weak field. Extrasolar planetary systems without close-in super-Earths may also have formed around weakly magnetized T Tauri stars. The strength of magnetic coupling may also evolve with the accretion rate in the disk (Kretke & Lin 2010). In a subsequent paper, we will address the magnetic coupling process that would play a key role in the origin of diversity of close-in super-Earths or Earths.

ACKNOWLEDGMENTS. We thank Micheal Mayor and Geoff Marcy for useful discussions. This work is supported by JSPS (20244013), NSFC(10233020), NCET (04-0468), NASA (NNX07A-L13G, NNX07AI88G, NNX08AM84G), JPL (1270927), and NSF(AST-0908807).

CORRESPONDENCE should be addressed to S. I. (ida@geo.titech.ac.jp).

Appendix. Prescription for eccentricity excitation and merging of embryos in post-oligarchic stage

We describe here prescriptions for embryos’ eccentricity excitations and merging process. Because giant impacts proceed after the depletion of disk gas and planetesimals, we consider only mutual gravitational interactions among the embryos and neglect damping forces from disk gas and dynamical friction from planetesimals.

The order of our procedures is:

- 1) set up initial conditions,
- 2) evaluate, for all pairs of embryos, the crossing time scale (τ_{cross}) over which sufficiently large eccentricities are excited (by their mutual secular perturbations) so that their orbits would cross each other,
- 3) evaluate the amount of eccentricity excitation (e) and semimajor axis change (δa) of embryos pairs which are destined to cross each other’s orbits next,
- 4) determine whether these changes may lead to the participating embryos to undergo secondary orbit crossings with any other neighboring embryos,
- 5) compute changes in the e and a for embryos which undergo secondary orbit crossings,
- 6) make adjustment in a for all embryos participated in orbit crossing so that their total orbital energy is conserved,
- 7) identify a pair of orbit-crossing embryos which are most likely to physically collide with each other,
- 8) create a merged embryo, and
- 9) repeat step 2, until τ_{cross} of embryo pairs exceed the system age.

The detailed prescriptions for each step are as follows:

1. The initial mass (m_j) and semimajor axis (a_j) of j th embryo are determined by oligarchic growth model (see section 2.6). The eccentricity (e_j) of dynamically isolated embryos are assigned randomly by a Rayleigh distribution with mean values of their Hill eccentricities (defined as $(m_j/3M_*)^{1/3}$ where M_* is the host star mass). Embryos’ initial eccentricities are of the order of 0.001-0.01. Since eccentricities are significantly excited by embryos’ mutual interaction after the onset of orbit crossing, the initial small values of e_j do not affect the results.
2. Given m_j, a_j , and e_j , the crossing time (timescales on which orbital crossing starts) of each pair (i, j) of the embryos are calculated, following the fitting formula obtained by Zhou et al.

(2007) with some slight modifications:

$$\log\left(\frac{\tau_{\text{cross}}}{T_{\text{K}}}\right) = A + B \log\left(\frac{b}{2.3r_{\text{H}}}\right), \quad (15)$$

where T_{K} is Keplerian time at the mean $a(= \sqrt{a_i a_j})$ of the pair, $b = |a_i - a_j|$, $r_{\text{H}} = ((m_i + m_j)/3M_*)^{1/3}a$, and

$$\begin{aligned} A &= -2 + e_0 - 0.27 \log \mu, \\ B &= 18.7 + 1.1 \log \mu - (16.8 + 1.2 \log \mu)e_0, \\ e_0 &= \frac{1}{2} \frac{(e_i + e_j)a}{b}, \\ \mu &= \frac{(m_i + m_j)/2}{M_*}. \end{aligned} \quad (16)$$

3. The pair with the shortest orbit crossing time (τ_{cross}^*) is assumed to undergo close encounters before any other pairs. During these close encounters, embryos' excited velocity dispersion is limited by surface escape velocity of the perturber $v_{\text{esc},j}$ (Safronov 1969; Aarseth et al. 1993). The corresponding eccentricity is

$$e_{\text{esc},ij} = \frac{v_{\text{esc},ij}}{v_{\text{K}}} = \frac{\sqrt{2G(m_i + m_j)/(R_i + R_j)}}{\sqrt{GM_*/a}} \simeq 0.28 \left(\frac{m_i + m_j}{M_{\oplus}}\right)^{1/3} \left(\frac{\rho}{3\text{gcm}^{-3}}\right)^{1/6} \left(\frac{a}{1\text{AU}}\right)^{1/2}, \quad (17)$$

where v_{K} is Keplerian velocity, and R_j is the physical radius calculated from m_j with bulk density ρ of 3 gcm^{-3} inside the ice line and 1 gcm^{-3} outside it. The eccentricity change is partitioned according to the mass of interacting bodies (Nakazawa & Ida 1988, 1989) and the eccentricity distribution is relaxed to a Rayleigh distribution (Ida & Makino 1992). Thus, the individual excited eccentricities are given by

$$e_j = \frac{m_i}{m_i + m_j} e_{\text{esc},ij} \mathcal{R}, \quad (18)$$

where \mathcal{R} is a random number produced by a Rayleigh distribution with the mean value of unity. Changes in the semimajor axis associated with the eccentricity excitation are assumed to be $\pm e_j a_j$. Sign of the change is chosen to ensure that orbital separation between the pair is widened after their orbit crossing.

4. Energy and angular momentum exchanges during the close encounters between any pair of orbit-crossing embryos may induce them to cross the orbits of other nearby embryos. We classify all the affected embryos by their overlapping (relative to the modified pair) radial excursion (epicycle amplitude) into closely interacting groups. These groups generally contain several (≥ 3) embryos. We assume that the most massive embryo in each group dominates the outcome of successive close encounters within the group. The characteristic post-encounter eccentricity (e_j) for all but the most-massive embryos is given by equation (18) in which i is used to represent the most massive embryos in the group. We also assume the post-encounter eccentricity of the most-massive embryo is determined mostly by the second-most-massive embryo.

In general, successive close encounters lead to radial diffusion of the orbit-crossing embryos. In our prescription, changes in embryos’ semimajor axis are given by values chosen $W_j e_j a_j$. The statistical weight W_j (which has a skewed distribution within a limited range between -1 and 1) is introduced to reflect the kinematic distribution of the orbit crossing embryos. If the total mass (M_{in}) of all the encountering embryos in the group inside a particular embryo’s orbit is more than that (M_{out}) outside it, its probability of orbital expansion would be larger than that of orbital decay. In order to simulate this effect, we introduce a parameter $f_j = C_j(M_{\text{in}} - M_{\text{out}})/(M_{\text{in}} + M_{\text{out}})$ and set $W_j = f_j + (1 - |f_j|) * R_j$ where R_j is a random number with a uniform distribution in the range of $[-1, 1]$. With the results of N-body simulations, we also calibrate the magnitude of a constant $C_j \sim 2/3$.

Finally, close-encounters also excite embryos’ inclination. Magnitude of the orbital inclinations in radian may be about half of that of eccentricities (Ida & Makino 1992). However, the orbital inclinations do not directly affect the condition for orbit crossing, we are not concerned with embryos’ inclinations in this paper.

5. After the relative changes in the semimajor axes of all the orbit crossing embryos have been evaluated, we renormalize their semimajor axes by a constant numerical factor so that the total orbital energy of all the embryos in the group is conserved. In general, the modification of the semimajor axes introduced by this renormalization procedure is less than a percent order. This simple algorithm does introduce artificial changes in the total angular momentum of the encountering embryos.

Although, with a more complicated non-uniform renormalization factor, we can also conserve the total angular momentum of all the embryos in the group, we opted to limit the degrees of freedom at the expense of a small change in the total angular momentum of the system. After multiple close encounters and merger events, the total departure from angular momentum conservation of the entire system is limited to within 10% in typical models.

6. Close encounters also leads to physical collisions. We assume all physical collisions are cohesive and lead to merger events. Among the embryos in the orbit crossing group, a colliding pair (k, l) is chosen. However, after the impulsive momentum changes during repeated close-encounters not every chosen pairs from this group would retain overlapping orbits. If the radial excursions of any chosen pair do not overlap, another pair would be chosen until all available candidates are exhausted. (For example, after a close encounter between embryos 1 and 2, the former may cross the orbits of embryos 3 and 4 whereas the latter may cross the orbits of embryos 3 and 5. If collisional candidates are chosen to be embryos 1 and 5, this pair would be rejected.)

In order to take into account various factors which contributes to the collisional probabilities, we select the appropriate embryos with a statistically weighted random number. N-body simulations show that collision frequency decreases with embryos’ semimajor axes (because Keplerian period is longer and embryos’ spatial density is lower at larger semimajor axis). We adopt a weighted collisional probability which is proportional to a^{-3} .

7. A merged embryo is created from each colliding pair. Since we neglect fragmentation and rebound, the merged embryo acquires the total mass of the colliding pair. In the direct N-body simulations, the center of inertia and the total momentum are conserved after each cohesive collision. In our prescription, we do not follow the exact location and kinematics of the merger product. Instead, we use conservation laws to determine orbital elements of the merged embryos.

In principle, a small fraction of orbital angular momentum is transformed into spin angular momentum after each collision. However, the spin angular momentum is usually negligible. Total kinetic energy of the colliding embryos is also not conserved, because the collision dissipates kinetic energy of the relative motion and the merging changes binding energy. However, if their velocity dispersions are smaller than their two-body surface escape velocity ($v_{\text{esc},kl}$), the collisional dissipation energy is approximately equal to the change in the binding energy. In practice, the total orbital energy of the colliding pair is approximately conserved during the collision as well as the total angular momentum.

Assuming the conservation of orbital energy, the semimajor axis of the merged body (a_{kl}) is given by

$$\frac{m_k + m_l}{a_{kl}} = \frac{m_k}{a_k} + \frac{m_l}{a_l}. \quad (19)$$

In the case of $e \ll 1$, it is difficult to accurately evaluate the eccentricity of the merged body from the angular momentum conservation. Here, we assume that after each collision, the mass-weighted total Laplace-Runge-Lenz vector is conserved. This assumption holds for collisions between embryos with nearly circular Keplerian motion (*i.e.* $e \ll 1$) (Nakazawa & Ida 1988, 1989). In this limit, the eccentricity of the merged body (e_{kl}) is given by

$$\begin{aligned} (m_k + m_l)e_{kl} \cos \varpi_{kl} &= m_k e_k \cos \varpi_k + m_l e_l \cos \varpi_l, \\ (m_k + m_l)e_{kl} \sin \varpi_{kl} &= m_k e_k \sin \varpi_k + m_l e_l \sin \varpi_l, \end{aligned} \quad (20)$$

where ϖ 's are longitudes of periastron at the collision.

Due to the secular perturbation between orbit-crossing embryos, ϖ_k and ϖ_l generally precess independently over all angles. In principle, both longitudes can be chosen with uniformly distributed random phase (between 0 and 2π). However, even with overlapping regions of radial excursion, the orbits of a pair of eccentric embryos would only cross each other if the relative angle between their longitudes of periastron ($\theta = \varpi_k - \varpi_l$) is within some limited range. For example, eccentric embryos would not cross each other's orbits if their longitudes of periastron are aligned with $\theta \simeq 0$. In contrast, orbit crossing generally occurs between embryos with θ in some limited range centered at 180 degrees, provided $e_k a_k$ and $e_l a_l$ are larger than $|a_k - a_l|$.

In our prescription, we randomly generate a value of ϖ_l between 0 and 2π . We assume secular perturbation generally induces the longitudes of periastron of any pairs of embryos with overlapping orbits to precess and circulate so that their θ can always enter into the range ($\Delta\theta$) which allows them to collide. We first compute the magnitude of $\Delta\theta$ with independent

Keplerian orbits for the neighboring embryos. We then take into account that embryos' gravitational perturbation on each other tends to slightly broaden this range. The value of θ at the collision is randomly chosen from a value within the range $\Delta\theta$. The value of ϖ_k is then specified by ϖ_l and θ . Since the preferred value for θ is $\sim \pi$, the summation in the r. h. s. of eq. (20) usually results in cancellation, so that e_{kl} is often significantly smaller than e_k and e_l .

8. For updating the system time, we need to take into consideration 1) the time interval for neighboring embryos to cross each other's orbits ($\tau_{\text{cross}} = \tau_{\text{cross}}^*$ in equation 15) and that required for embryos to collide with each other τ_{collide} . Before each collision, embryos with overlapping orbits undergo repeated close scattering as θ circulates in and out the range of $\Delta\theta$. The magnitude of τ_{collide} for embryos with overlapping orbits is determined by their area filling factor (see Paper I). N-body simulations indicate that at a fraction of AU, $\tau_{\text{collide}} \sim 10^{5.5} - 10^{6.5} T_K$ for Earth-size embryos.

For pairs with moderately large initial separation ($b \gtrsim 5r_H$), $\tau_{\text{cross}} \gg \tau_{\text{collide}}$ and it is adequate to update the evolution of the system from t to $t + \tau_{\text{cross}}^*$. Pairs with small initial separation ($b \lesssim 5r_H$) are closely packed with wide range of $\Delta\theta$. Since it takes longer for them to collide than to cross each other's orbit, we update the evolution with a randomly generated τ_{collide} which has a uniform distribution in the range $(10^{5.5} - 10^{6.5})T_K$. Thus, the new system time is given by $t + \tau_{\text{cross}}^*$ for $\tau_{\text{cross}}^* > 10^{5.5}T_K$ and $t + \tau_{\text{collide}}^*$ otherwise.

After some collisional events, it is possible for the merger product to become dynamically isolated from all other embryos in the group. N-body simulations also indicate that following other cohesive collisions, several additional merger events may follow in rapid succession. For example, in a group of 4 orbit-crossing embryos, embryos 1 and 2 may merge first. The newly formed embryo may attain a new orbit which continues to overlap those of embryos 3 and 4. In that case, it is possible for the newly merged embryo to subsequently coagulate with embryos 3 or 4 or both. In order to take these possibilities into account, we repeat step 2 to 7 for all group members after each merger event, until their τ_{cross}^* (including the collisional lag time) has exceeded the integration time.

In step 7, we indicate that the merger product attains an eccentricity (e_{kl}) which is often significantly smaller either than e_k and e_l . This apparent eccentricity damping is due to the effect that merger events can only occur for a limited range between the longitude of periastron of the colliding embryos. Consequently, embryos' asymptotic eccentricities are usually smaller than e_{esc} . This inference is consistent with the results of previous N-body simulations (Kokubo et al. 2006).

In the prescription presented here, the only free empirical parameters are i) the weighted changes in the semimajor axis in step 4 and ii) the broadened range of $\Delta\theta$ in step 6. All the other procedures are based on fundamental dynamics although some of their efficiencies are approximated. The weighted a changes and the broadening of the phase range are also qualitatively based on celestial mechanics. The quantitative parameters for these processes are determined by

comparison with the results obtained by N-body simulations (Kokubo et al. 2006). Note that the same parameters are applied for all models in the present paper and we do not individually carry out fine tuning for different disk conditions.

REFERENCES

- Aarseth, S. J., Lin, D. N. C., Palmer, P. L. 1993, *ApJ*, 403, 351
- Artymowicz, P. 1993, *ApJ*, 419, 166
- Baruteau, C. & Lin, D. N. C. 2010, *ApJ*, 709, 759
- Beckwith, S. V. W. & Sargent, A. I., 1996, *Nature*, 383, 139
- Bodenheimer, P., & Pollack, J. B. 1986, *Icarus*, 67, 391
- Bodenheimer, P., Hubickyj, O. & Lissauer, J. J. 2000, *Icarus*, 143, 2
- Bryden, G. et al. 2009, *ApJ*, 705, 1226
- Chambers, J. E., Wetherill, G. W., Boss, A. P. 1996, *Icarus*, 119, 261
- Chiang, E. I. & Goldreich, P. 1997, *ApJ*, 490, 368
- Cieza, L. & Balibar, N. 2007, *ApJ*, 671, 605
- Cumming, A., Butler, R. P., Marcy, G. W., Vogt, S. S., Wright, J. T., Fischer, D. 2008, *PASP*, 120, 531
- Duncan, M. J. & Levison, H. F. 1997, *Science*, 276, 1670
- Fischer, D. A. & Valenti, J. A. 2005, *ApJ*, 622, 1102
- Garaud, P. & Lin, D. N. C. 2007, *ApJ*, 654, 606
- Goldreich, P. & Lynden-Bell, D. 1969, *ApJ*, 156, 59
- Goldreich, P., & Tremaine, S. 1982, *ARA&A*, 20, 249
- Goldreich, P., Lithwick, Y. & Sari, R. 2004, *ARA&A*, 42, 549
- Greaves, J. S., Fischer, D. A., Wyatt, M. C., Beichman, C. A., & Bryden, G. 2007, *MNRAS*, 378, L1
- Haisch, K. E., Lada, E. A. & Lada, C. J. 2001, *ApJ*, 553, L153
- Hasegawa, M. & Nakazawa, K. 1990, *A&A*, 227, 619
- Hayashi, C. 1981, *Prog. Theor. Phys. Suppl.*, 70, 35
- Herbst, W. & Mundt, R. *ApJ*, 633, 967
- Ida, S. & Makino, J. 1992, *Icarus* 96, 107

- Ida, S. & Lin, D. N. C. 2004, *ApJ*, 604, 388 (Paper I)
- Ida, S. & Lin, D. N. C. 2004, *ApJ*, 616, 567 (Paper II)
- Ida, S. & Lin, D. N. C. 2005, *ApJ*, 626, 1045 (Paper III)
- Ida, S. & Lin, D. N. C. 2008a, *ApJ*, 673, 487 (Paper IV)
- Ida, S. & Lin, D. N. C. 2008b, *ApJ*, 685, 584 (Paper V)
- Ikoma, M., Nakazawa, K. & Emori, E. 2000, *ApJ*, 537, 1013
- Ikoma, M., Emori, E. & Nakazawa, K. 2001, *ApJ*, 553, 999
- Iwasaki, K., Emori, H., Nakazawa, K. & Tanaka, H. 2002, *PASJ*, 54, 471
- Kato, M. T., Nakamura, K., Tandokoro, R., Fujimoto, M. & Ida, S. 2009, *ApJ*, 691, 1697
- Kennedy, G. M., Kenyon, S. J. & Bromley, B.C. 2006, *ApJ*, 650, L139
- Kennedy, G. M. & Kenyon, S. J. 2008, *ApJ*, 682, 1264
- Kenyon, S.J. & Bromley, B.C. 2004, *ApJ*, 602, 133
- Kleine, T., Munker, C., Mezger, K., Palme, H., 2002, *Nature*, 418, 952
- Kokubo, E. & Ida, S. 1996, *Icarus*, 123, 180
- . 1998, *Icarus*, 131, 171
- . 2002, *ApJ*, 581, 666
- Kokubo, E., Kominami, J. & Ida, S. 2006, *ApJ*, 642, 1131
- Koller, J., Li, H. & Lin, D. N. C. 2003, *ApJ*, 596, L91
- Kominami, J. & Ida, S. 2002, *Icarus*, 157, 43
- Konigl, A. 1991, *ApJ*, 370, L39
- Kretke, K. A. & Lin, D. N. C. 2007, *ApJ*, 664, L55
- Kretke, K. A., Lin, D. N. C., Garaud, P. & Turner, N. J. 2009, *ApJ*, 690, 407
- Kretke, K. A. & Lin, D. N. C. 2010, in preparation
- Laine, R. O., Lin, D. N. C. & Dong, S. 2008. *ApJ*685, 521
- Laine, R. O. & Lin, D. N. C. 2010, in preparation
- Laughlin, G., Steinacker, A. & Adams, F.C. 2004. *ApJ*608, 489

- Lecar, M., Podolak, M., Sasselov, D. & Chiang, E. 2006, *ApJ*, 640, 1115
- Li, H., Lubow, S. H., Li, S. & Lin, D. N. C. 2009, *ApJ*, 690, 52
- Lin, D. N. C., Bodenheimer, P. & Richardson, D. 1996, *Nature*, 380, 606
- Lin, D. N. C. & Papaloizou, J. C. B. 1985, *Protostars and Planets II*, ed. D. C. Black & M. S. Matthews (Tucson: Univ. of Arizona Press), 981
- Lin, D. N. C., & Papaloizou, J. C. B. 1993, in *Protostars and Planets III*, ed. E. H. Levy and J. I. Lunine (Tucson: Univ. of Arizona Press), 749
- Lissauer, J. 1987. *Icarus*, 69, 249
- Lynden-Bell, D. & Pringle, J. E. 1974, *MNRAS*, 168, 603
- Mardling, R.A. & Lin, D.N.C. 2004, *ApJ*, 614, 955
- Masset, F. S., Morbidelli, A., Crida, A. & Ferreira, J. 2006, *ApJ*, 703, 857
- Masset, F. S. & Casoli, J. 2009, *ApJ*, 703, 857
- Mayor, M. *et al.* 2009, *A&A*, 507, 487
- McNeil, D., Duncan, M. & Levison, H. 2005. *AJ*, 130, 2884
- Marzari, F. & Weidenschilling, S. 2002, *Icarus*, 156, 570
- Mizuno, H. 1980. *Prog. Theor. Phys.*
- Mordasini, C., Alibert, Y. & Benz, W. 2009. *A&A*, 501, 1161
- Murray, C. D. & Dermott, S. F. 2000, *Solar System Dynamics*, Cambridge University Press
- Nagasawa, M., Lin, D.N.C., & Thommes, E. 2005, *ApJ* 635, 578
- Nakazawa, K. & Ida, S. 1988. *Prog. Theor. Phys. Suppl.* 96, 167
- Nakazawa, K. & Ida, S. 1989. *A&A*, 220, 293
- Nelson, R.P. 2005. *A&A*, 443, 1067
- O'Brien, D., Morbidelli, A. & Levison, H. F. 2006, *Icarus*, 184, 39
- Ogihara, M. & Ida, S. 2009. submitted
- Ogihara, M., Duncan, M. & Ida, S. 2010, submitted
- Paardekooper, S.-J., Baruteau, C., Crida, A. & Kley, W. 2009, *MNRAS*, 401, 1950

- Pan, M. & Sari, R. 2005, *Icarus*, 173, 342
- Pollack, J. B., Hollenbach, D., Beckwith, S., Simonelli, D. P., Roush, T., & Fong, W. 1994, *ApJ*, 421, 615
- Pollack, J. B., Hubickyj, O., Bodenheimer, P., Lissauer, J. J., Podolak, M., & Greenzweig, Y. 1996, *Icarus*, 124, 62
- Rebull, L. M., Stauffer, J. R., Megeath, S. T., Hora, J. L. & Hartmann, L. 2006, *ApJ*, 646, 297
- Safronov, V. 1969, *Evolution of the Protoplanetary Cloud and Formation of the Earth and Planets* (Moscow: Nauka Press)
- Shakura, N. I. & Sunyaev, R. A. 1973, *A&A*, 24, 337
- Schlaufman, K. C., Lin, D. N. C. & Ida, S. 2009, *ApJ*, 691, 1322
- Schlaufman, K. C., Lin, D. N. C. & Ida, S. 2010, submitted
- Shu, F., Najita, J., Ostriker, E., Wilkin, F., Ruden, S. & Sunasa, L. *ApJ*, 429, 781
- Stewart, G. R. & Ida, S. 2000, *Icarus*, 143, 28
- Stewart, S. T. & Leinhardt, Z. M. 2009, *ApJ*, 691, L133
- Takeuchi, T. & Artymowicz, P. 2001, *ApJ*, 557, 990
- Tanaka, H., Takeuchi, T. & Ward, W. 2002, *ApJ*, 565, 1257
- Tanaka, H. & Ward, W. 2004, *ApJ*, 602, 388
- Terquem, C. & Papaloizou, J. C. B. 2007, *ApJ*, 654, 1110
- Thommes, E. W., Matsumura, S. & Rasio, F. A., 2008, *Science*, 321, 814
- Thommes, E., Nagasawa, M., & Lin, D.N.C., 2008, *ApJ*676, 728
- Udry, S. & Santos, N. C. 2007, *ARA&A*, 45, 397
- Ward, W. 1986, *Icarus*, 67, 164
- Ward, W. 1993, *Icarus*, 106, 274
- Wyatt, M. C. 2008, *ARA&A*, 46, 339
- Yin, Q. et al. 2002, *Nature*, 418, 949
- Zhou, J., Lin, D. N. C. & Sun, Y. 2007, *ApJ*, 666, 423

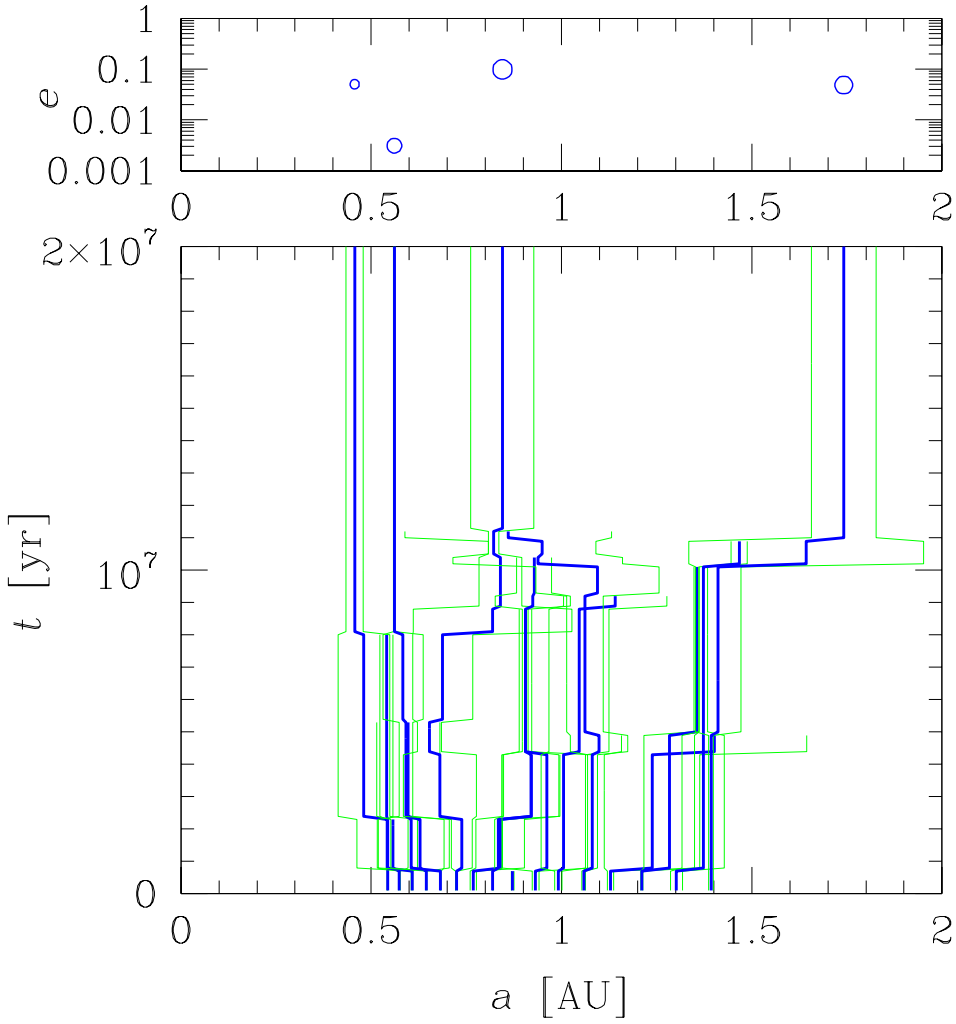


Fig. 1.— An example of evolution of embryos in the post-oligarchic stage calculated by the semi-analytical model. Initially, 16 embryos are placed in the disk with $f_d = 1$. Thick and thin lines in the lower panel represent the evolution of embryos’ semimajor axes and peri/apo-centers respectively. Discontinuities in lines represent merger events for embryos with others. The upper panel shows semimajor axes and eccentricities of final planets. The radii of circles are proportional to physical sizes.

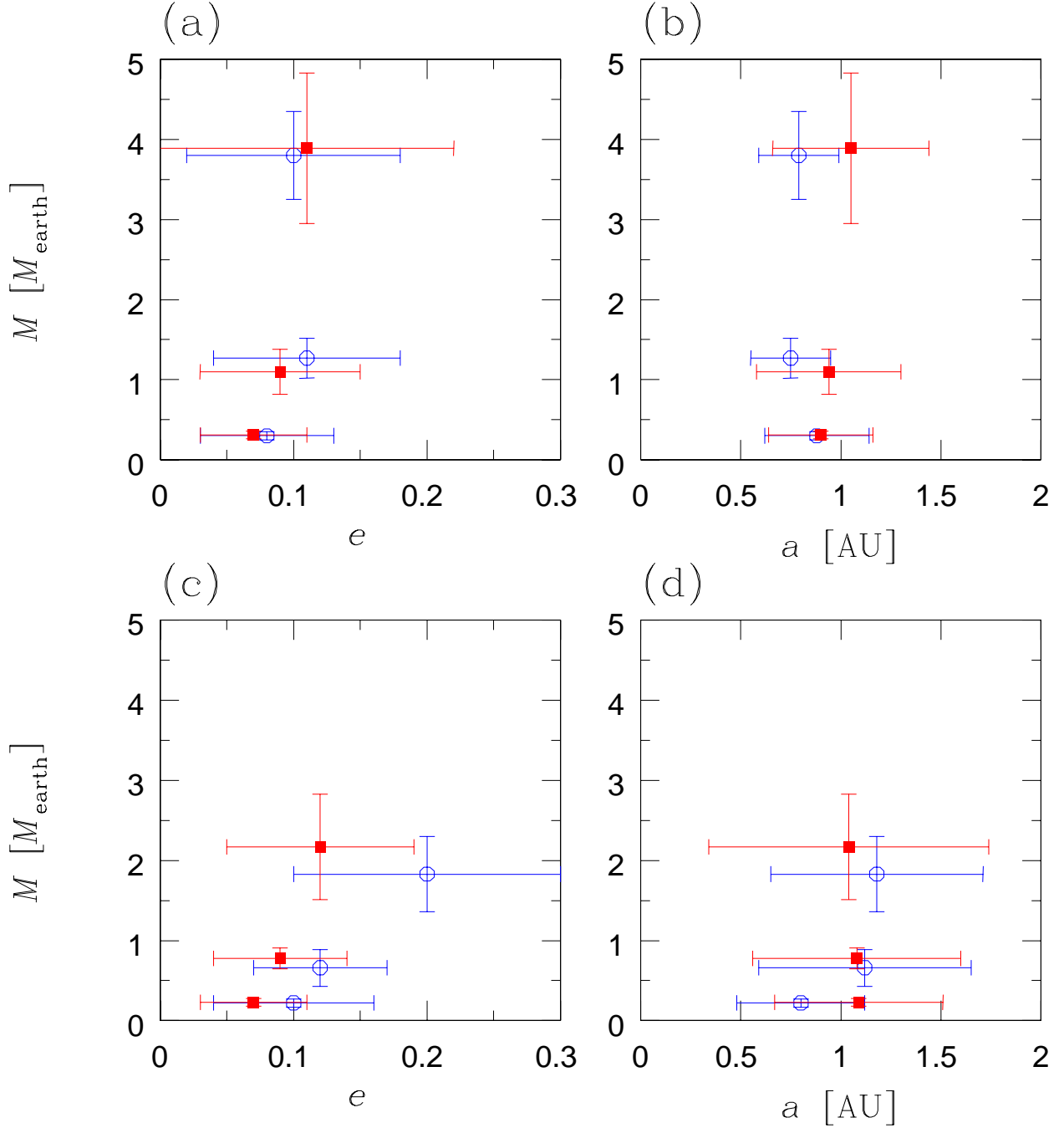


Fig. 2.— The averaged quantities of 20 models obtained by our semi-analytical model are represented with filled squares. For comparison purpose, the results of N-body simulations of Kokubo et al. (2006) are represented with open circles. The bars indicate standard deviations. (a) orbital eccentricity and mass of the most massive bodies, (b) their semimajor axis and mass, (c) orbital eccentricity and mass of the second most massive bodies, and (d) their semimajor axis and mass. the second most massive bodies (panels c and d). Results for three sets of disk parameters ($f_d = 0.3, 1$ and 3) are plotted. The average masses increase with f_d .

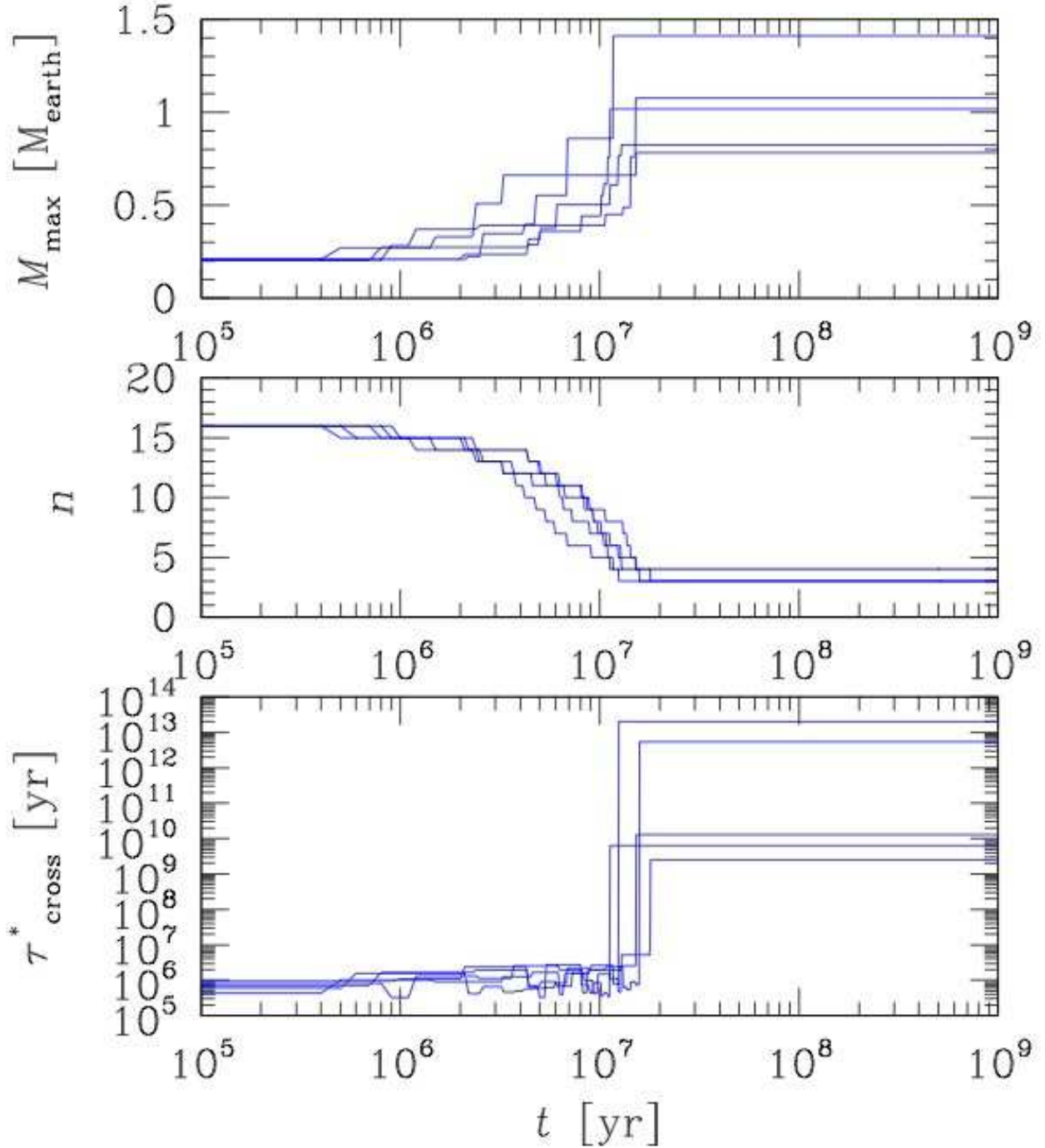


Fig. 3.— Time evolution of the mass of the most massive embryo (M_{\max}) is plotted on the top panel. The total number of residual embryos is plotted in the middle panel. The minimum orbit crossing time for any pairs of embryos is plotted in the bottom panel. Five sets of models (generated with different random number seeds) for $f_d = 1$ disks are presented here. Each model starts with 16 embryos at the onset of the simulation.

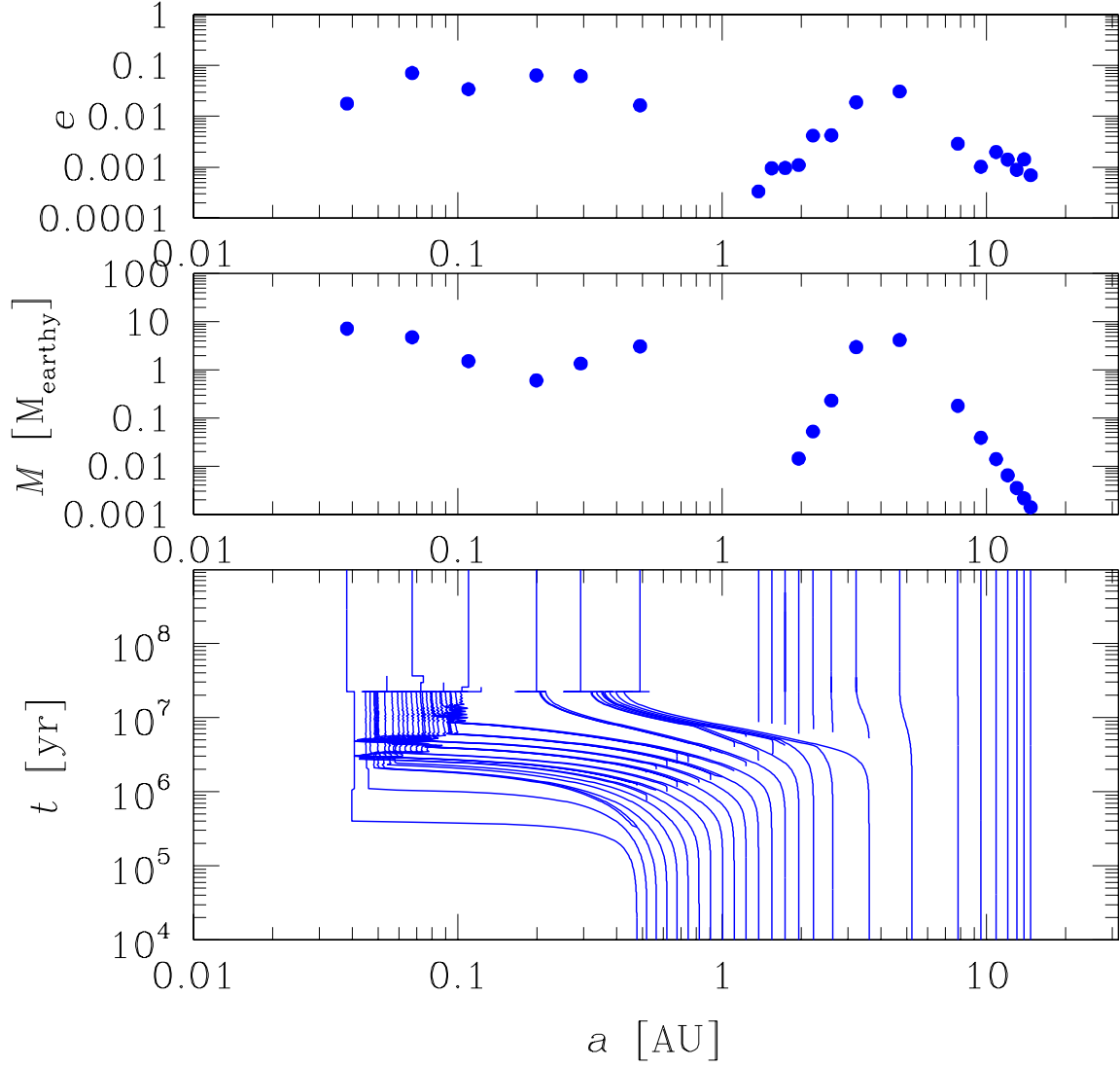


Fig. 4.— Time evolution of semimajor axes of all embryos is plotted in the bottom panel. The asymptotic (at 1 Gyr) eccentricities and masses of all “final” planets are plotted in the top and middle panels. In this model, we set $f_d = 2$. We also assume the presence of a disk cavity is sufficient to stall the inward migration of all embryos in the proximity of their host stars.

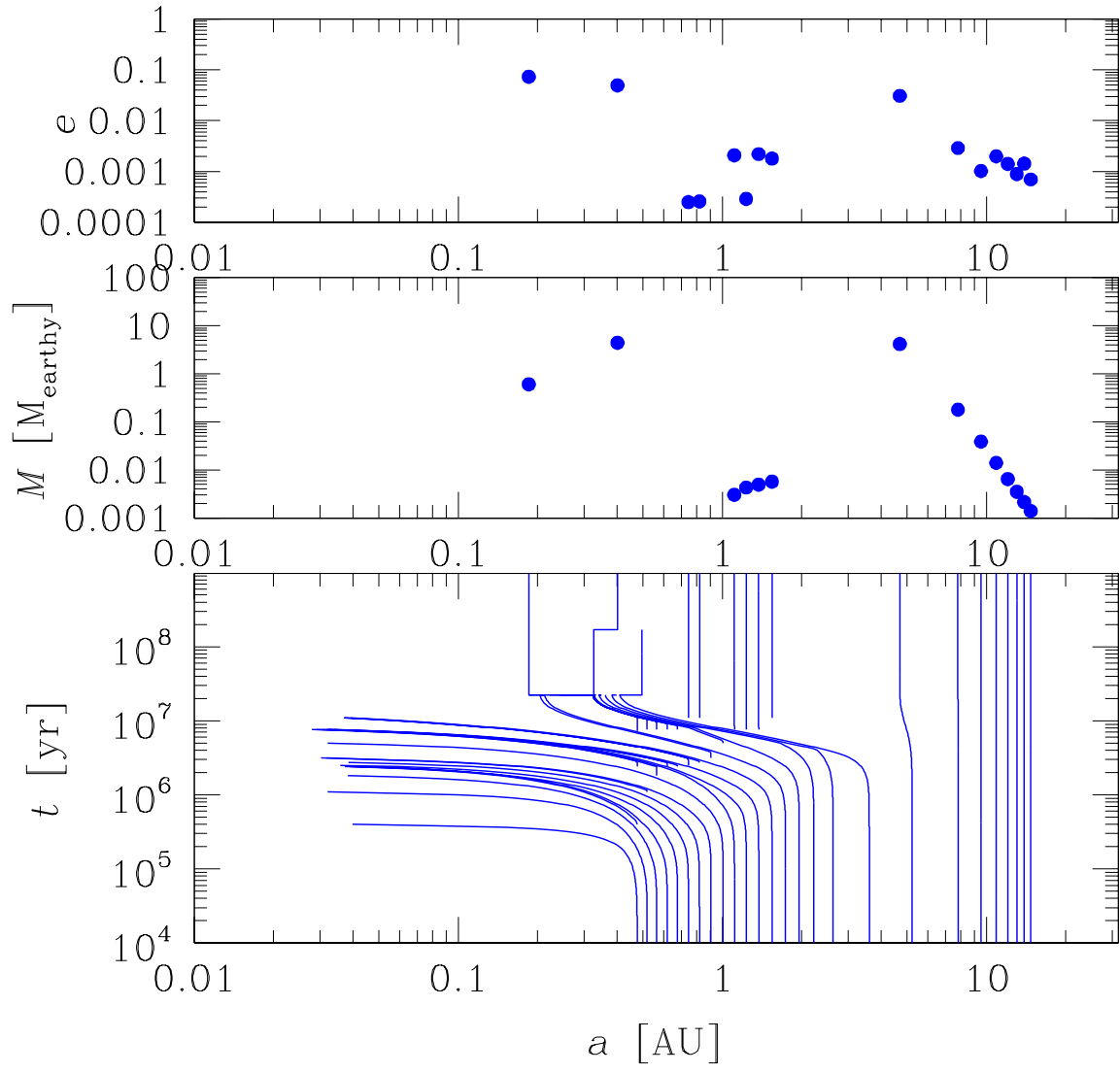


Fig. 5.— The same as figure 5 except we did not impose a migration barrier near the host star. In our prescription, we adopt the no-cavity condition for the inner boundary.

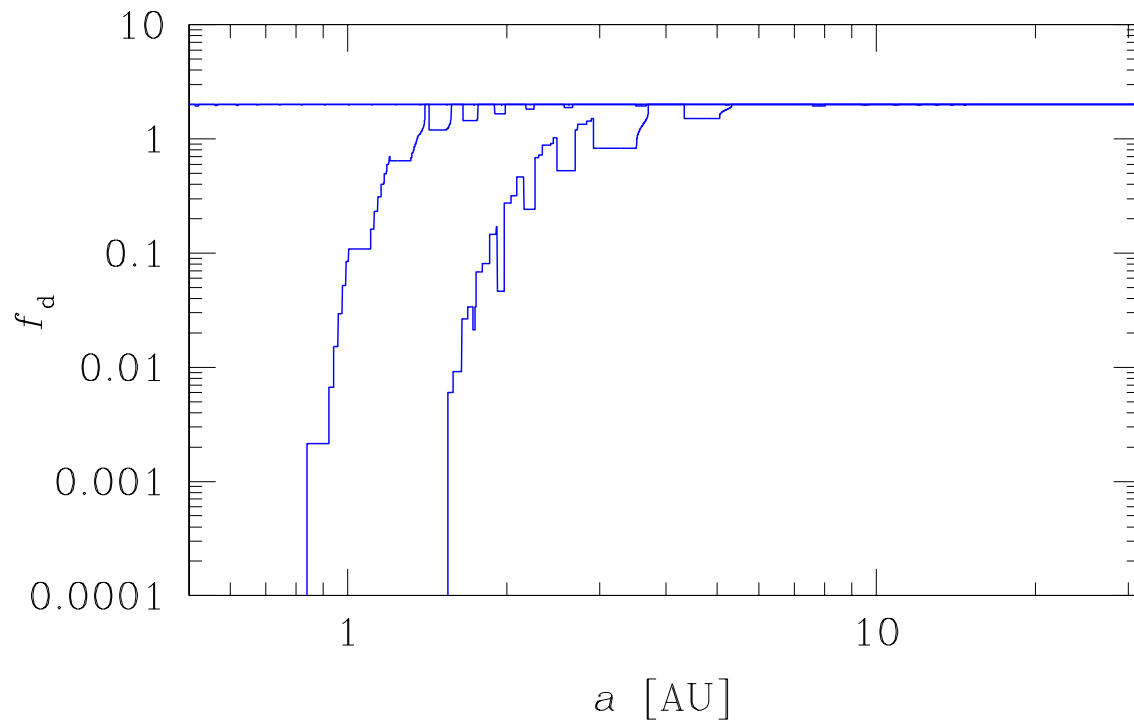


Fig. 6.— The time evolution of planetesimal surface density due to their accretion by embryos. Same model parameters are used as for the result in Figure 4. The distributions at $t = 0, 10^4, 10^6$ and 10^8 yrs are plotted (the lines at $t = 0$ and 10^4 yrs almost overlap with each other).

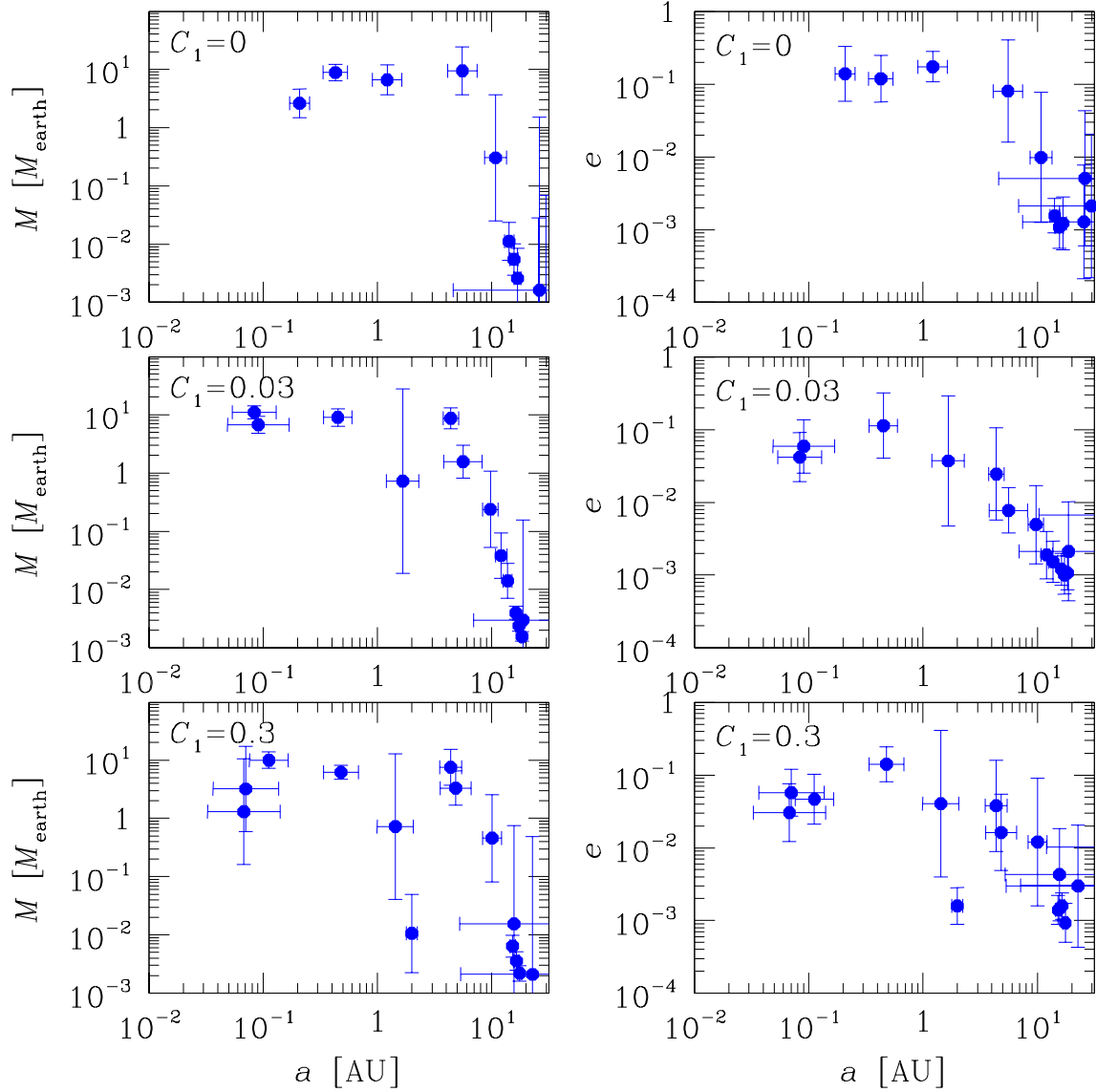


Fig. 7.— Simulated planetary systems for $C_1 = 0, 0.03$, and 0.3 are shown in the top, middle, and bottom panels respectively. These results are generated from models with $f_{d,0} = 3$. A migration barrier is imposed in accordance with the the cavity condition. The left and right panels show asymptotic masses and eccentricities of bone fide planets at $t = 1$ Gyr. The mean values of 20 runs are expressed by the symbols with bars of standard deviations.

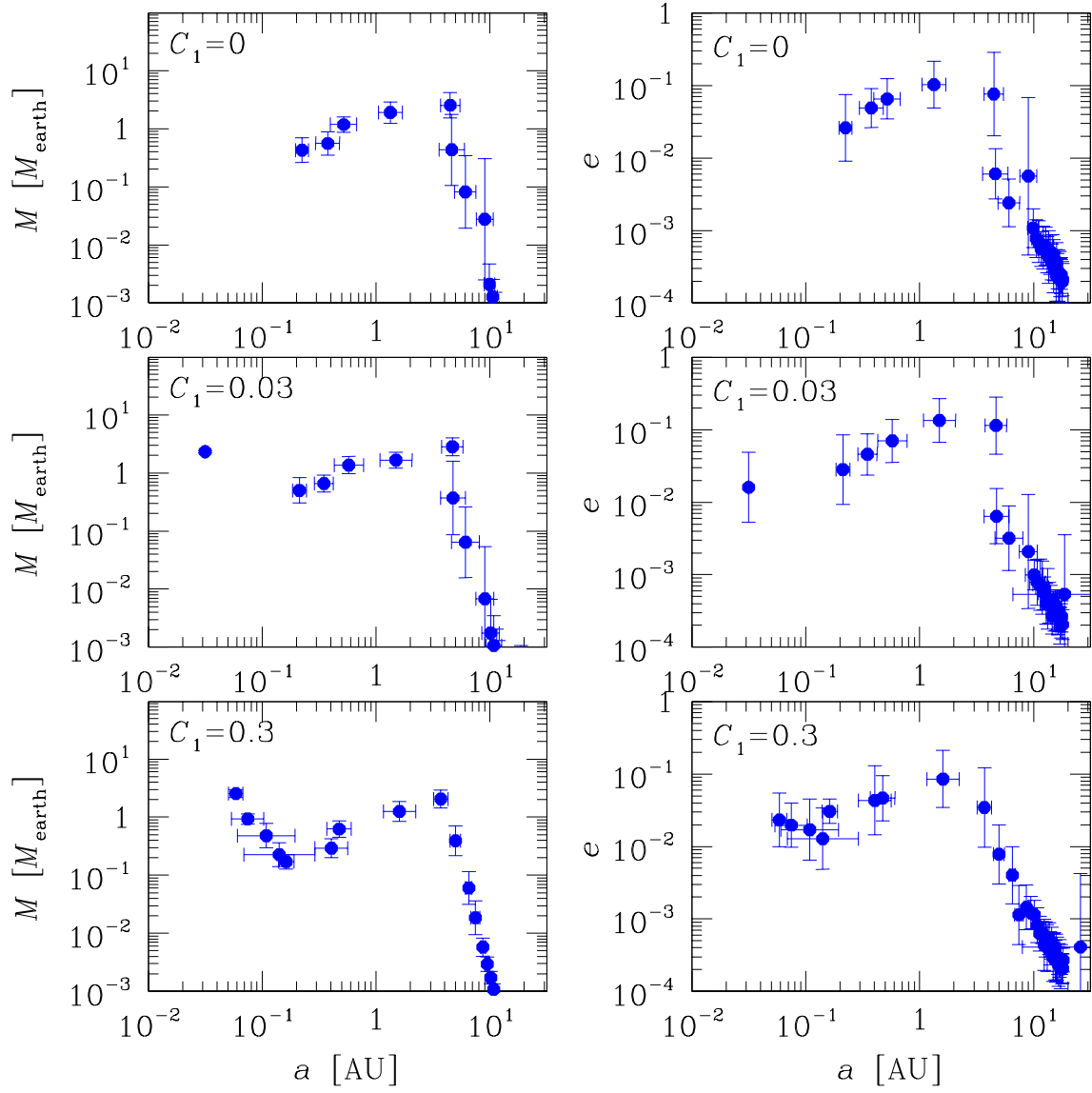


Fig. 8.— The same as Figures 7 except for $f_d = 1$.

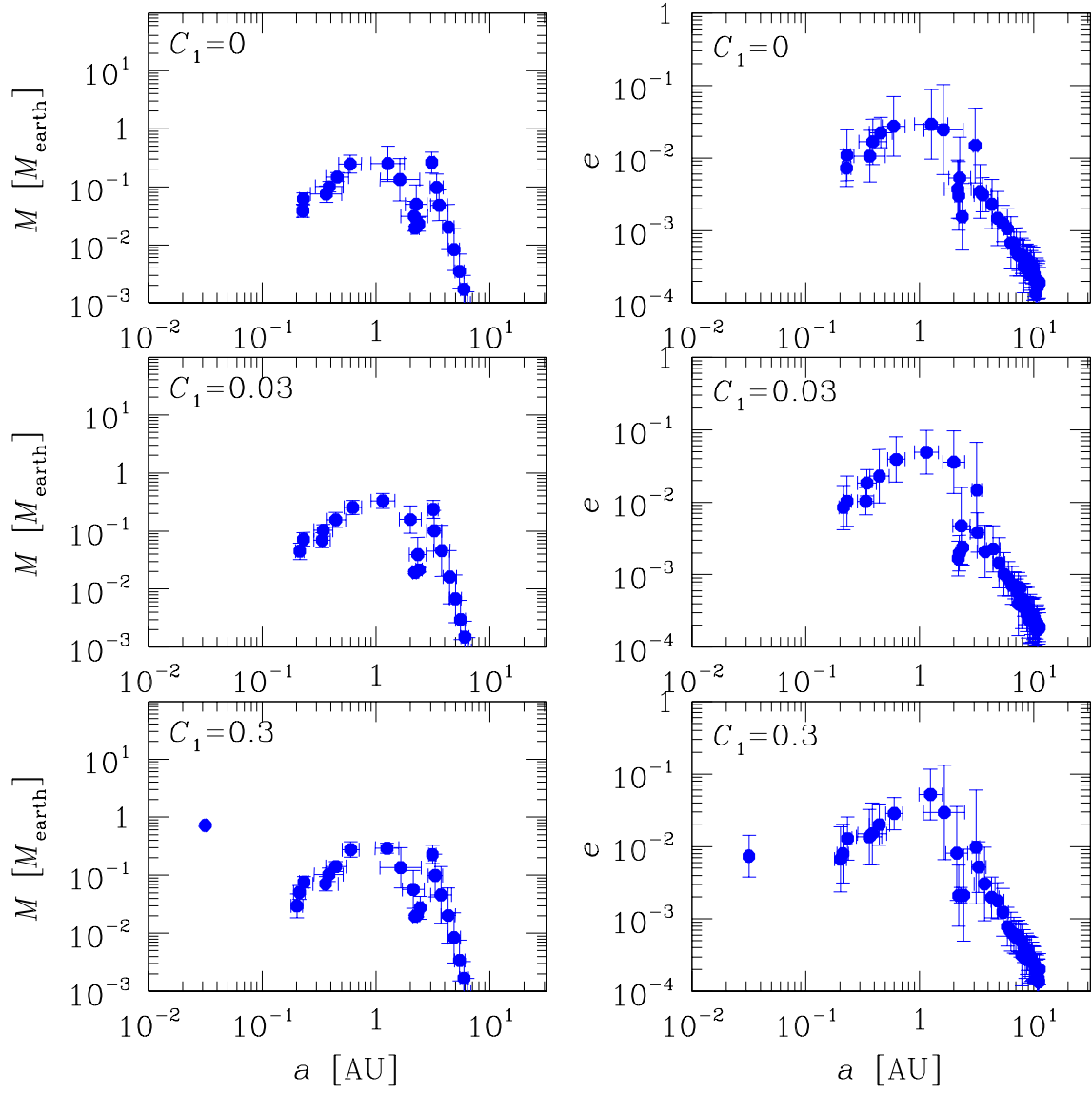


Fig. 9.— The same as Figures 7 except for $f_d = 0.3$.

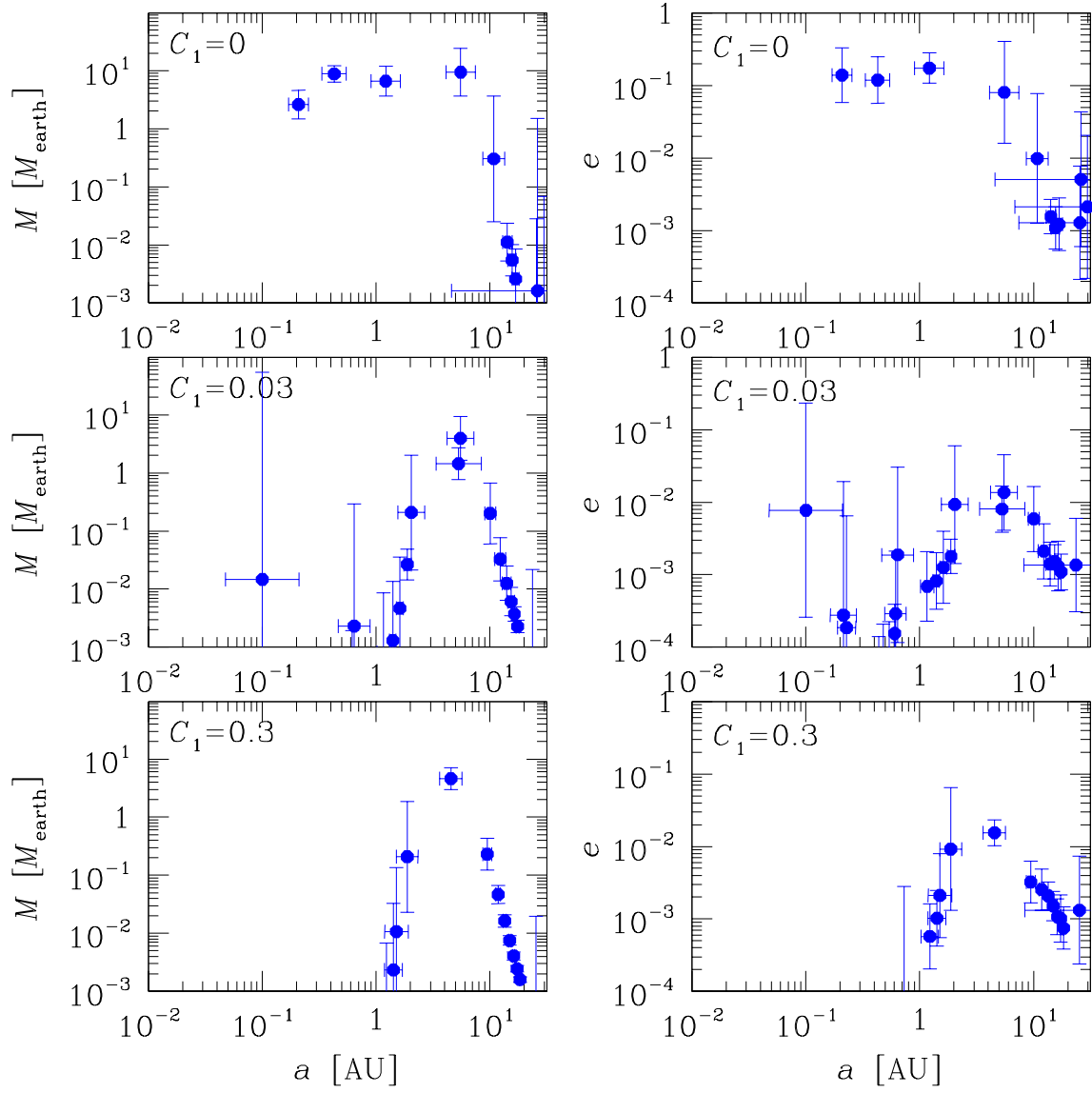


Fig. 10.— The same as Figures 7 except for the non-cavity condition.